Biosensors and Bioelectronics 143 (2019) 111617

Contents lists available at ScienceDirect

Biosensors and Bioelectronics

journal homepage: www.elsevier.com/locate/bios

Photodetectors based on two dimensional materials for biomedical application

Shuangjie Liu[a], Xiao-dong Zhang[a,b,*], Xiaosong Gu[a], Dong Ming[a,**]

[a] Tianjin International Joint Research Center for Neural Engineering, Academy of Medical Engineering and Translational Medicine, Tianjin University, Tianjin, 300072, China

[b] Tianjin Key Laboratory of Low Dimensional Materials Physics and Preparing Technology, Institute of Advanced Materials Physics, School of Sciences, Tianjin University, Tianjin, 300350, China

ARTICLE INFO

Keywords:
Photodetector
2D materials
Biomedical application
Wearable/implantable devices

ABSTRACT

Mobile medical devices provide great promise for self-health monitoring and preventive medicine. Especially, photodetectors (PDs) based on two-dimensional (2D) materials have attracted the wide interest in biomedicine and healthcare. In this review, we summarized the research progress of PDs based on 2D materials, and described the important applications of these devices in the wearable and implantable devices. We also analyzed their various properties such as sensitivity, mechanical flexibility, robustness and biocompatibility of the wearable and implantable devices. The typical biomedical application, such as UV-radiation monitor, pulse oximeters and retinal prosthesis were reviewed. We also discussed some of the technical challenges in wearable and implantable device and possible solutions. The state of art, non-invasive devices show great promising for real-time pathological monitor, health management and tracking.

1. Introduction

Breakthroughs in fundamental science often follow from advances in technology and methodology. PDs convert the absorbed optical signals into measurable electrical signals, which are of central importance to many applications (Dhanabalan et al., 2016; Buscema et al., 2015; Xu et al., 2016a; Lin et al., 2017), such as optical communications, biomedical imaging and environmental monitoring. At the same time, 2D materials have received wide attention in the field of optoelectronic devices thanks to the excellent photoelectric and structural properties (Chitara et al., 2011a; Wang et al., 2015a; Zhang et al., 2016a). More recently, the research on PDs has mainly focused on the fabrication of devices using various 2D optoelectronic materials (Zeng et al., 2018; Chen et al., 2018; Li et al., 2017a; Mingjin et al., 2018; Wang et al., 2018; He et al., 2019; Long et al., 2019). To date, through various optimization measures such as preparing a hybrid structure of heterojunctions, not only can the light absorption capacity of the device be enhanced, but also the detection spectrum range can be extended to ultraviolet (UV) to infrared and even terahertz bands (Long et al., 2019; Lu et al., 2019; Cao et al., 2019; Vellampatti et al., 2019; Yang et al., 2019). The performance of PDs based on 2D materials has achieved impressive results, and the performance has been continuously improved, including responsivity, detectivity and spectral response range (Alsaif et al., 2019; Tian et al., 2019; Liu et al., 2019a). Hence, the wide band, ultra-sensitive and ultra-fast response photoelectric detection is realized. 2D materials, such as graphene and transition metal dichalcogenides (TMDs), have greatly improved atomic utilization compared with bulk materials. Through thickness control and element doping, the band structure and optoelectronic properties can be more easily controlled. One of the advantages of 2D materials is the excellent mechanical strength, flexibility and high transparency, which has an attractive prospect in the fields of wearable intelligent devices and flexible energy storage devices. Therefore, PDs based on 2D materials have been gradually studied and applied in wearable and implantable biomedical fields.

The growing demand for more effective, specific and safer treatment methods in the biomedical domain has broadened the horizons of the research and turned it to more innovative therapies. Technologies that combine electronic components with the human body are now able to restore function and monitor health conditions (Schwartz et al., 2013; Gao et al., 2015; Wang et al., 2014). However, conventional PDs contain rigid, flat and fragile semiconductor wafers as supporting

* Corresponding author. Tianjin International Joint Research Center for Neural Engineering, Academy of Medical Engineering and Translational Medicine, Tianjin University, Tianjin, 300072, China.

** Corresponding author.

E-mail addresses: xiaodongzhang@tju.edu.cn (X.-d. Zhang), richardming@tju.edu.cn (D. Ming).

https://doi.org/10.1016/j.bios.2019.111617
Received 20 June 2019; Received in revised form 6 August 2019; Accepted 19 August 2019
Available online 21 August 2019
0956-5663/ © 2019 Elsevier B.V. All rights reserved.

substrates, thereby limiting the ways the devices are used. To some extent, the research applied in biomedical field is pushed by the potential alternative application of integrating thin film devices on flexible substrates. It is worth noting that if the PDs are applied to biomedical fields, such as retinal prosthesis, electronic skin and even pulse oximeter, higher requirements are put forward for the device including flexibility, robustness, stability and biocompatibility. These characteristics provide the possibility for the application of the device in biomedicine.

The attractive capabilities and related research advances of modern wearable biosensors have been highlighted in several recent reviews (Kim et al., 2019; Heikenfeld et al., 2019; Jin et al., 2017; Yang and Gao, 2018; Sabu et al., 2019), with a focus on the wearable biosensors for minimally invasive or non-invasive measurements of analytes in biological fluids. Unlike wearable biosensors, the PDs reviewed here for biomedical applications, provide an overview of health monitoring and disease regulating by recognizing physiologically relevant indicators. Non-invasive wearable PDs avoids painful and dangerous blood sampling procedures, monitor health through real-time continuous physiological information, and alert users or medical staff for disease prevention. As a highly sensitive optical sensor, the implantable PDs can be used to detect the optical signals inherent in living brain tissue to prevent and diagnose diseases. Despite rapid progress in photodetection technology over the past few years, we are only at the beginning of understanding how wearable and even implantable photodetection technologies can improve health and performance. Past research and progress have paved the way for future wearable and implantable photodetection technologies, enabling real-time pathology monitoring, health management and tracking in the biomedical fields for a wide range of healthcare applications.

In the following review, we outline an overview of the key advances in 2D material-based PDs in the biomedical fields and discuss the potential of the wearable and implantable devices in biomedical applications. First, we introduce various properties of flexible PDs based on 2D materials, including robustness, stability and biocompatibility, indicating their potential for successful application in biomedical applications. Pioneering studies of the invasive and non-invasive PDs that have had a major impact on the biomedical field were subsequently reviewed. Finally, we discuss the importance and future direction of wearable and implantable PDs in the biomedical field, highlighting existing bottlenecks and presenting insights into the prospects of this exciting research area.

2. PDs based on photoelectric materials

2.1. PDs based on graphene

Graphene is a monatomic-thick 2D system, comprising carbon atoms arranged in a hexagonal honeycomb lattice (Li et al., 2017b), as shown in Fig. 1a. Since the key advance in graphene synthesis was explored in 2004 (Novoselov et al., 2004), it has attracted wide interest in terms of the graphene-based photodetection devices due to its numerous attractive electronic, optical, mechanical and thermal properties (Patil et al., 2013; Echtermeyer et al., 2014; Chitara et al., 2011b; Withers et al., 2013; Guo et al., 2016; Fang et al., 2017; Li and Zhu, 2016). For instance, it has broad spectrum absorption characteristics from UV to far infrared, ultra-high carrier mobility at room temperature, very large surface area, good mechanical flexibility and excellent biocompatibility (Novoselov et al., 2004; Wang et al., 2008), which have gained extensive research in physics, chemistry and industry (Echtermeyer et al., 2014; Chitara et al., 2011b; Withers et al., 2013; Hossain et al., 2017a; Liu et al., 2015a). Additionally, the high mobility of electrons and holes in graphene can greatly improve the response speed of infrared detectors and exhibit an attractive prospect for development of ultra-fast infrared detectors. However, unlike conventional semiconductor materials, pristine single- and few-layer graphene materials have no band gap (Craciun et al., 2011; Khodkov et al., 2012), which leads to low responsivity and photoelectric efficiency. Thus, the performance of such graphene-based PDs is greatly limited by weak light absorption and low responsivity. Much effort has been devoted to improve the optoelectronic properties of graphene materials and to optimized the performance of graphene-based PDs (Craciun et al., 2011; Khodkov et al., 2012; Ohta et al., 2006; Li et al., 2008). One strategy is to functionalize graphene through materials engineering such as creating band gap in graphene by doping, using graphene oxide (GO), reduced GO (RGO), shaping graphene to nanoribbons (GNR), and so on (Ohta et al., 2006; Li et al., 2008; Chang et al., 2010, 2013; Shen et al., 2013). The responsivity of PDs based on RGO and GNR is ~10 times and ~3 times higher than that of the ordinary graphene devices, respectively (Chitara et al., 2011b). Another effort to achieve high-performance has focused on the development of graphene hybrid structure such as graphene/semiconductors (Hossain et al., 2017a; Zhang et al., 2014b; Li et al., 2016), graphene/polymer (Bao et al., 2010) or graphene/quantum dots (QDs) (Konstantatos et al., 2011; Liu et al., 2014a; Yu et al., 2016). To date, a variety of 2D semiconductor materials have been used to form heterojunction photodiodes with graphene, such as Ti_2O_3 (Yu et al., 2018; Cheng et al., 2019), $MoTe_2$ (Yu et al., 2017; Li et al., 2019a), MoS_2 (Xu et al., 2018a; De et al., 2016; Hua et al., 2014), WS_2 (Tan et al., 2016), and ZnO (Dang et al., 2015; Duan et al., 2017; Liu et al., 2015b; Boruah et al., 2015, 2016).

As shown in Fig. 1b, the Si QDs/graphene/Si PDs are fabricated (Yu et al., 2016), and Si QDs on the top of graphene cause the built-in potential of the graphene/Si Schottky junction to increase. Both of the electrical and optical contributions of Si QDs enable us to demonstrate graphene/Si Schottky-junction PDs with record-high responsivity of ~0.495A/W (Fig. 1c), record-short response time of < 25 ns, and excellent specific detectivity of $\sim 7.4 \times 10^9$ Jones. Fig. 1d demonstrated a hybrid $MoTe_2$/graphene PD in which multilayer $MoTe_2$ acts as the photoactive layer, and monolayer graphene as a highly efficient pathway for photocarriers as well as an encapsulation layer (Yu et al., 2017). The device achieved a high responsivity of ~970.82 A/W (at 1064 nm) and broadband photodetection (visible ~ 1064 nm), as shown in Fig. 1e. Moreover, flexible devices based on the $MoTe_2$/graphene heterostructure on flexible substrate also retains an excellent photodetection ability after thousands of times bending test (1.2% tensile strain) (the **inset** of Fig. 1f), with a high responsivity of ~60 A/W at 1064 nm at V_{DS} = 1 V (Fig. 1f), which provides a promising platform for highly efficient, flexible, and low cost broadband NIR PDs. Fig. 1g demonstrates the PD with high responsivity in the mid-infrared regime using the hybrid graphene/Ti_2O_3 structures (Yu et al., 2018), achieving a responsivity of 300 A/W in a broadband wavelength range up to 10 μm (Fig. 1h). It hinges upon the highly efficient broadband absorption of Ti_2O_3 nanoparticles and the fast carrier transport in graphene, which shows ~2 orders of magnitude higher than that of the commercial mid-infrared PDs. The PD based on gold-patched graphene nano-stripes (the **inset** of Fig. 1i) shows an ultra-broad bandwidth with high-responsivity ranging from 0.6 A/W at wavelength of 800 nm to 8 A/W at 20 μm (Fig. 1i), which has the ultra-wide photodetection bandwidth with the ultra-high responsivity due to the use of gold-patched graphene nanostripes.

2.2. PDs based on layer 2D TMDs

In addition to graphene, very recently, other 2D materials, usually indicated by graphene-like 2D materials, are also emerged as important materials in electronics and optoelectronics (Zhu et al., 2015; Gupta et al., 2015; Zhu et al., 2017; Xu et al., 2013; Sun and Chang, 2014; Chiu and Xu, 2017). Specifically, promising graphene-like 2D materials, such as hexagonal boron nitride (h-BN) nanosheets, layered transition metal dichalcogenides (TMDs), and transition metal oxides, show 2D structures similar to graphene but have much different electronic and optical properties. In addition, due to the distinct properties and high

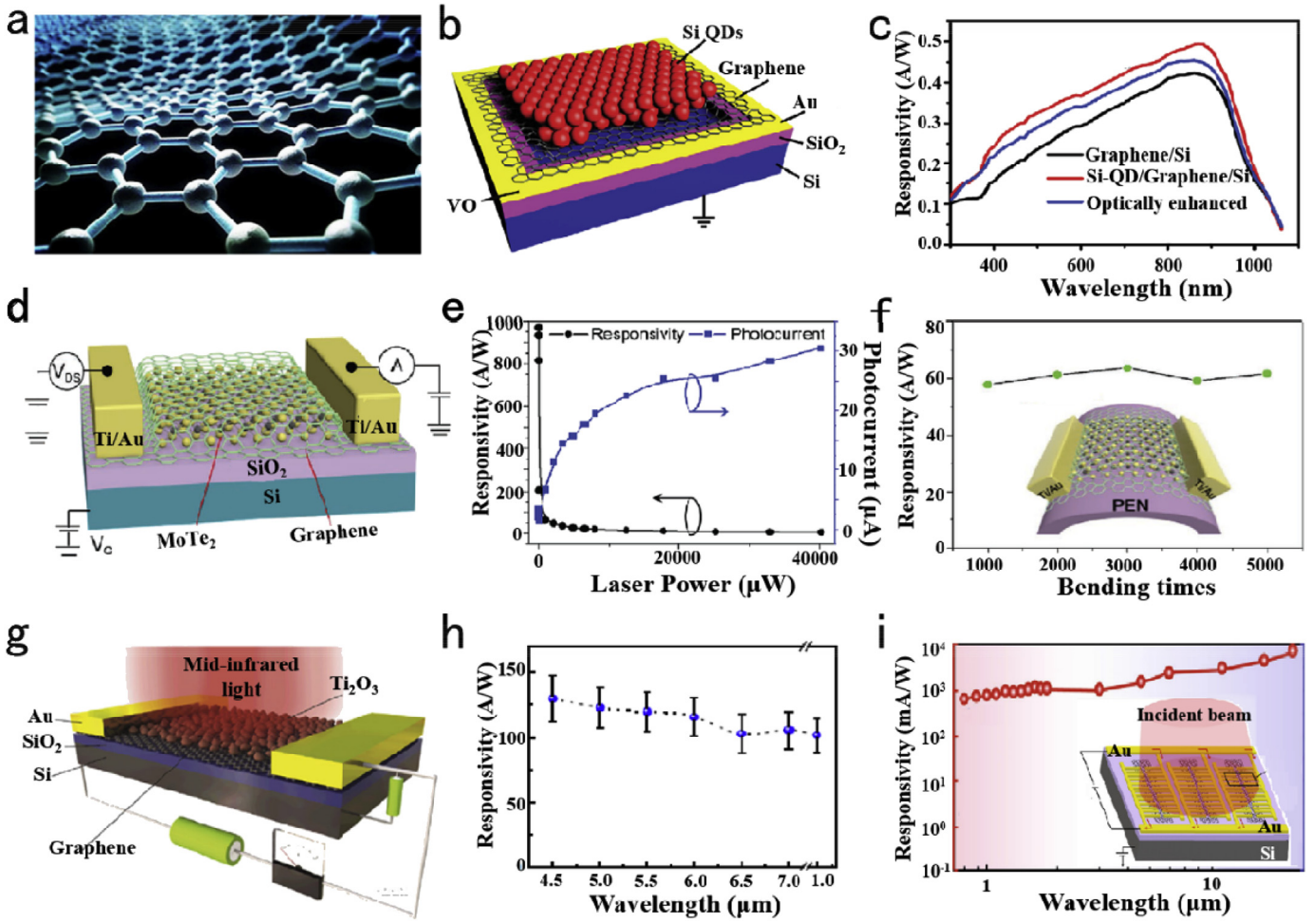

Fig. 1. (**a**) The structure diagram of graphene. (**b**) Schematic diagram of a typical Si-QDs/graphene/Si PD. (**c**) Responsivity of the graphene/Si and Si-QD/graphene/Si PDs under the bias of −1 V. (**d**) Schematic diagram of the $MoTe_2$/graphene PD. (**e**) Responsivity and photocurrent versus incident light power at 1064 nm of the $MoTe_2$/graphene PD. (**f**) Responsivity versus bending times under the same illumination condition (1064 nm, 112.3 μW). **Inset**: Schematic diagram of the device after bending. (**g**) Schematic diagram of hybrid graphene/Ti_2O_3 nanoparticle PD. (**h**) Responsivity versus different illumination wavelengths in the mid-infrared regime of the hybrid graphene/Ti_2O_3 PD. (**i**) Responsivity of the PD at an optical power of 2.5 μW and bias voltage of 20 mV. **Inset**: Schematic diagram of a PD based on gold-patched graphene nano-stripes. (For interpretation of the references to colour in this figure legend, the reader is referred to the Web version of this article.)

specific surface areas, these 2D materials are important in various applications such as optoelectronics, catalysts, chemical and biological sensors and other specific applications (Zhu et al., 2017; Chen et al., 2015a; Liu et al., 2019b; Pumera and Loo, 2014; Yang et al., 2013). Recently, PDs based on graphene-like 2D materials, especially layered TMDs such as MoS_2, WSe_2, GaTe, WS_2 and their nanocomposites, have received widespread attention for their special electronic structure (Li and Zhu, 2016; Liu et al., 2016; Jariwala et al., 2017; Novoselov et al., 2016; Ajayan et al., 2016; Hafeez et al., 2016; Kang et al., 2015). It is worth noting that, the band structures of 2D TMDs is different from that of bulk crystals. As the material becomes thinner from the bulk to monolayer, the band structure of TMDs would transform from the indirect band gap to direct band gap due to quantum confinement effects (Yun et al., 2012; Kuc et al., 2011). And it also has a mobility of as high as 200 cm^2/V with an on-off ratio of about 10^8 at room temperature, all showing a great potential for optoelectronic applications.

MoS_2, as a typical 2D layered metal chalcogenide, has been widely investigated for the excellent structure and optoelectronic properties (Zhang et al., 2017; Kwak et al., 2016; Sun et al., 2016; Li et al., 2017c; Zhao et al., 2017; Velický et al., 2016). MoS_2 is cheap and shows an electron mobility comparable to silicon, which is suitable for the optoelectronic devices. It has also been found that the photoluminescence of single layer structure is much better than that of multilayer structure (Tongay et al., 2013; Splendiani et al., 2010), which shows that the excellent optoelectronic property of 2D layered structure of single layer. Unlike optoelectronic devices based on gapless graphene, MoS_2 can freely control the switches of devices, which will show the wide application prospect in many fields such as new photoelectric detection and sensing (Geim and Grigorieva, 2013).

Initially, PD based on monolayer MoS_2 is prepared (Fig. 2a), and it exhibits high responsivity up to 880 A/W (Fig. 2b) due to the direct band gap (Oriol et al., 2013). Recently, several strategies have been developed to improve the performance of MoS_2 PDs (Zhang et al., 2016b; Wang et al., 2015b, 2017; Tan et al., 2017; Huo et al., 2017; Xiao et al., 2018; Wen et al., 2016; Gomathi et al., 2017; Pak et al., 2018; Huang et al., 2018; Ding et al., 2018). For example, a vertical multilayered n-MoS_2/n-Si homotype heterojunction PD (Fig. 2c) is fabricated by Zhang and his colleagues (Zhang et al., 2016b), which exhibits excellent responsivity up to 11.9 A/W and high detectivity of 2.1×10^{10} Jones. It is worth noting that the device shows a high-speed response rise time of 30.5 μs, as well as a small fall time of 70.6 μs (Fig. 2d), remarkably faster than those reported for MoS_2-based PDs. Afterwards, PD with an ultra-thin p-GaTe/n-MoS_2 van der Waals p-n junction structure was constructed, as shown in Fig. 2e. The p-n junction shows strong gate- and temperature-tunable rectification characteristics and photovoltaic effects. As a result, it achieves a

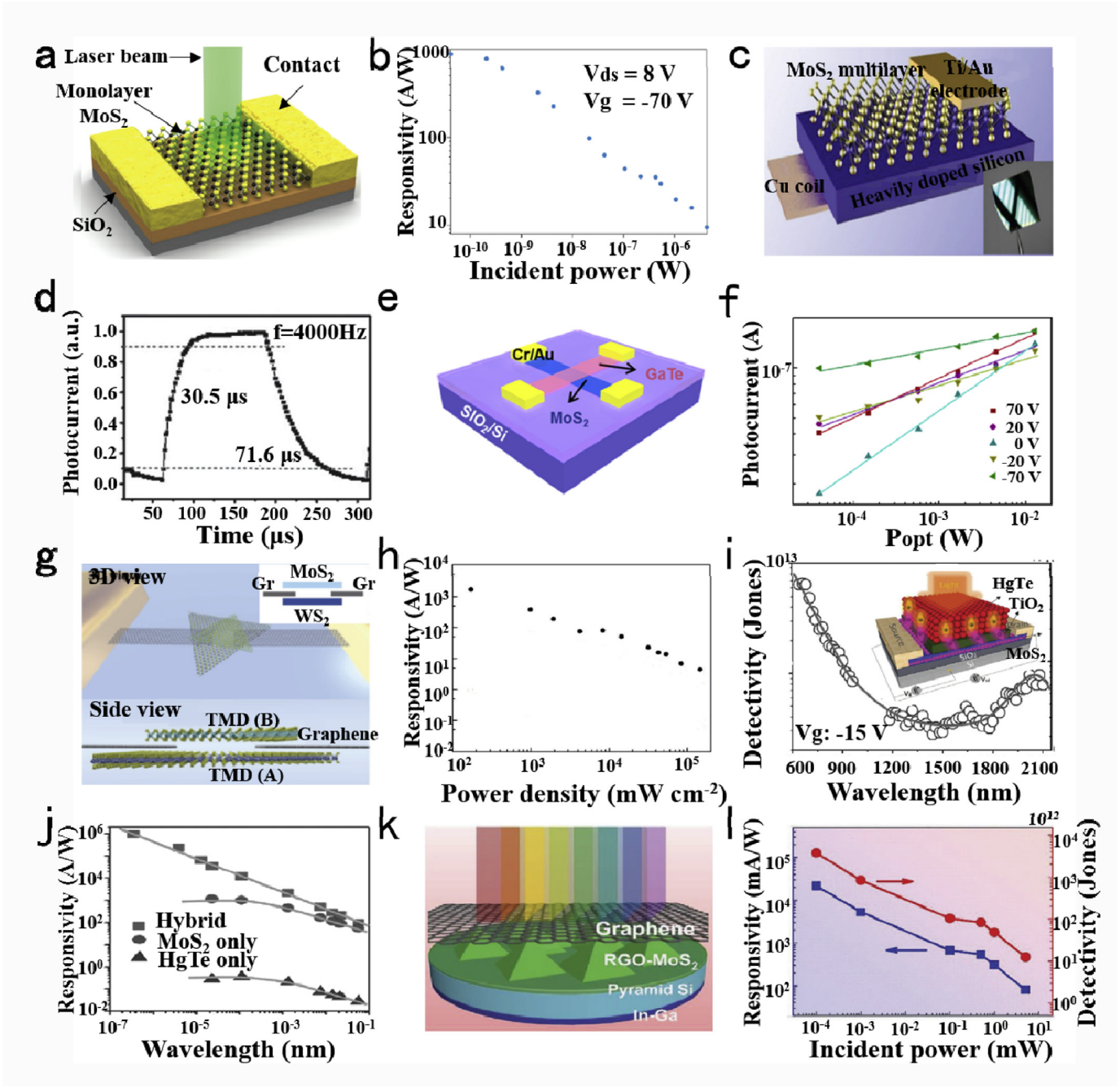

Fig. 2. (**a**) 3D schematic view of the single-layer MoS_2 PD. (**b**) Responsivity versus incident power of the MoS_2 PD. (**c**) Schematic diagram of the vertical multilayered MoS_2/Si heterojunction. (**d**) Time response characteristics of the heterojucntion under different pulsed light illumination (650 nm, ≈ 90 mW cm^{-2}). (**e**) Schematic of the GaTe/MoS_2 van der Waals p−n junction PD. (**f**) Photocurrents under various light intensities with different gate voltages. (**g**) Schematic 3D and side views of Graphene–WS_2/MoS_2–Graphene PD. (**h**) Responsivity versus irradiation power. (**i**) Wavelength dependence of the measured detectivity (at 1 Hz modulation frequency). The inset is the schematic diagram of the MoS_2/TiO_2/HgTe hybrid PDs. (**j**) Wavelength dependence of the responsivity of MoS_2, HgTe and hybrids PDs, respectively. (**k**) Schematic diagram of the 3D RGO–MoS_2/pyramid Si heterojunction PD. (**l**) The responsivity and detectivity versus the light power.

response of up to 21.8 A/W and a high detectivity of 8.4×10^{13} Jones (Fig. 2f). The photoresponse can be greatly enhanced by using the type-II band alignment of vertically stacked WS_2/MoS_2 semiconducting heterobilayers (Fig. 2g), as recently reported by Tan and his colleagues (Tan et al., 2017). With this unique design, the device shows significantly improved responsivity - by ~2 orders of magnitude - to 10^3 A/W compared with monolayer devices of WS_2 and MoS_2, as shown in Fig. 2h. The improvement of performance is due to the strong Coulomb interaction between WS_2 and MoS_2 layers. Huo et al. demonstrated hybrid 2D QD PD based on MoS_2 and HgTe QDs (the **inset** of Fig. 2i). (Huo et al., 2017) The detectivity is ~10^{12} Jones (Fig. 2i) in the short-wave infrared of 2 μm and responsivity up to 10^6 A/W under a weak optical power density of 0.35 μW cm^{-2} (Fig. 2j). Lately, a structurized 3D heterojunction of RGO–MoS_2/pyramid Si (Fig. 2k) is demonstrated (Xiao et al., 2018), and in the device, the Si pyramid structure improves optical absorption, the imperfect crystallinity narrows the band gap of MoS_2 and the inserted RGO enhances charge separation/transportation. As a results, the hybrid PD shows excellent performance with a responsivity of 21.8 A/W and extremely ultra-high detectivity of 3.8×10^{15} Jones (Fig. 2l).

2.3. PDs based on metal oxide semiconductors

Metal oxide semiconductors, including ZnO and TiO_2, have become popular materials in UV PDs owing to their unique optoelectronic properties (Fang et al., 2011; Ning et al., 2018a; Leung et al., 2018; Li et al., 2019b). Metal oxide semiconductor nanostructures with large surface-to-volume ratio can significantly increase the number of surface trap states and prolong the lifetime of photo-generated carriers (Devan et al., 2012), which leads to the high photoconductive gain and responsivity of the PDs. On the one hand, these surface effects reduce the response speed of PDs due to the slow oxygen adsorption/desorption process on the metal oxide semiconductor surface (Hsu et al., 2012). On the other hand, the optical absorption is limited in the UV region because of the wide band gap in nature. Both limit their application in photoelectric detection. In order to break the trade-off between improving responsivity and increasing spectral response range, several strategies have been proposed, including the development of novel PD structures (Schottky barrier (Zhang et al., 2016c; Patel et al., 2017; Zhu et al., 2018) and heterojunction (Chong et al., 2015; Ouyang et al., 2017, 2018)), surface modification, and construction of specific geometric structures.

A broadband PD was fabricated by spinning perovskite ($MAPbI_3$) QDs on TiO_2 nanotubes (NTs) array (Fig. 3a), which realize photodetection range from UV to full visible spectrum (Zheng et al., 2017). Compared with pure TiO_2 PDs, the sensitivity of heterostructure devices is enhanced by ~3 orders of magnitude in the visible range (Fig. 3b). Moreover, the detectivity of heterostructure can reach $\sim 10^{11}$ Jones in the visible range as shown in Fig. 3c. When was exposed to moist air for 72 h or heated to 100 °C, it was found that the optoelectronic performance hardly decayed (Fig. 3d and e), demonstrating the excellent stability. Then a novel self-powered UV PD based on ZnO homojunction was prepared by simply connecting pure ZnO and Ag-doped ZnO nanofibers to form p-n junction (Ning et al., 2018b). The device shows a high responsivity of 1×10^3 μA/W and can simultaneously realize a relatively short rise/decay time of 3.90 s/4.71 s (Fig. 3f). Thus it can achieve a perfect balance between sensitivity and response time due to the Schottky contact between Ag metal and ZnO. Afterwards, fiber-shaped ZnO/graphene PDs based on Schottky junction are constructed (Zhu et al., 2018), as shown in Fig. 3g. The device exhibits excellent performance with responsivity as high as 1.92 A/W due to the combination of the interface and strain engineering. Moreover, the responsivity enhances by 12.5% under −0.33% compressive strain (Fig. 3h), which was attributed to the high Schottky barrier height. Recently, high performance bismuth oxychloride (BiOCl) nanosheets/TiO_2 nanotube arrays heterojunction UV PDs have been prepared (Fig. 3i). (Ouyang et al., 2018) The heterojunction in the BiOCl nanosheets are beneficial to the separation of photo-generated carriers and regulate the transmission of electrons, thus improving the optoelectronic performance of the device. As can be observed from Fig. 3j and k, the device simultaneously achieves the high responsivity of 41.94 A/W, the high detectivity of 1.41×10^{14} Jones and the ultra-fast decay speed of 0.81 s. These results demonstrate that the rational design of the novel heterojunctions show great potential for improving the performance of PDs.

2.4. PDs based on black phosphorus (BP)

As a novel 2D layered semiconductor material, BP exhibits high carrier mobility (1000 $cm^2V^{-1}s^{-1}$) (Liu et al., 2014b), anisotropic optoelectronic properties (Ling et al., 2016), tunable direct band gap (Yuan et al., 2015; Zhang et al., 2014a) and high on/off ratios (Li et al., 2014), thus it is considered as one of the ideal materials for manufacturing high-performance PDs (Buscema et al., 2015; Poya et al., 2015; Weinan et al., 2015; Chen et al., 2015b). Following the first report of broadband BP-based PDs using few-layer of BP sheets (Buscema et al., 2014), 2D heterostructure p-n diodes (Yuan et al., 2015; Deng et al., 2014) and chemically modified BP-based PDs (Xiang et al., 2015) were constructed, resulting in continuous improvement of device performance.

Xu et al. reported that selenium-doped BP, it was found that optoelectronic performance shows ~20 times higher than that of original BP (Xu et al., 2016b). Despite the great achievements of BP-based PD, the stability of BP is still a serious challenge. Afterwards, Ren et al. have prepared self-powered PDs based on large-sized 2D BP nanosheets (Ren et al., 2017), as shown in Fig. 4a, which exhibit preferable responsivity and environmental robustness under light irradiation (Fig. 4b and c). The excellent photoresponse performance was from excellent durability of BP nanosheets in a specific KOH solution. To further improve the responsivity and detectivity, Ye et al. demonstrated broadband PD using a vertical photogate heterostructure BP-on-WSe_2 (Ye et al., 2017), as shown in Fig. 4d. The responsivity can reach up to $\sim 10^3$ A/W and $\sim 5 \times 10^{-1}$ A/W respectively, and the detectivity can reach up to $\sim 10^{14}$ and $\sim 10^{10}$ Jones respectively in visible and infrared light (Fig. 4e). These high performances suggest that the PDs based on photogate structure provide an opportunity for infrared detection. At present, the integration of silicon-on-insulator waveguides with BP-based PDs (Fig. 4f) were realized by Huang and his colleagues (Huang et al., 2019). At the bias of 1 V, the BP-based PD achieved a responsivity of 23 A/W and 2 A/W at 3.68 μm and 4 μm, respectively (Fig. 4g), which is the ultra-high among the waveguide-integrated IR detectors.

3. Biomedical applications

3.1. Wearable biomedical PDs

At present, medical concepts begin to favor active prevention, early diagnosis and treatment of diseases. The large-scale medical equipment used in hospitals obviously cannot meet the daily physical sign monitoring, so wearable intelligent health monitoring equipment came into being. Wearable medical PDs may play an important role in reducing the cost of medical care. The thin film electronic device tightly attached to the skin is equipped with electronic components for health monitoring and information technology. When the electronic device is worn, the mechanical flexibility and stretching ability of the thin film device helps to minimize stress and discomfort associated with wearing because of their compliance and flexibility. The demand for wearable optoelectronic technology in biomedicine is increasing, which requires innovative technologies to fabricate flexible, compact and wearable high-performance PDs.

Solar radiation, especially UV radiation, is closely related to human life. A reasonable dose of UV radiation is beneficial for vitamin D synthesis and bone development. Excessive UV radiation intake will cause skin aging, wrinkles and even skin cancer in severe cases (Narayanan et al., 2010; Araki et al., 2016; Kim et al., 2016a). Therefore, real-time monitoring of UV radiation can reasonably utilize UV rays and prevent skin diseases caused by excessive UV exposure. Wearable UV PDs can monitor UV radiation in real time and protect human health. An et al. prepared a highly flexible PD based on RGO-ZnO (An et al., 2018) (Fig. 5a). The device can be conformably attached to skin and monitor UV rays. Through photocurrent response to multiple UV on/off cycles (Fig. 5b), the device shows consistent and repeatable output current and indicates good response recovery performance. By further patterning the bendable mica substrate, the device is bent by 0°, 90° and 180°, respectively (Fig. 5c). It is found that even if it is bent to 180°, there is only a very slight current drop (Fig. 5d), proving the mechanical flexibility and stability of the device. Excellent flexibility allows it to be in close contact with human hands and used as a wearable PD for health monitoring. The photocurrent still hardly drops after 500 bending-unbending cycles with the bending angle of 180° (Fig. 5e), indicating the excellent mechanical stability and reliability, which is essential for wearable PDs.

Subsequently, Xu et al. prepared a wearable, fiber-shaped and self-

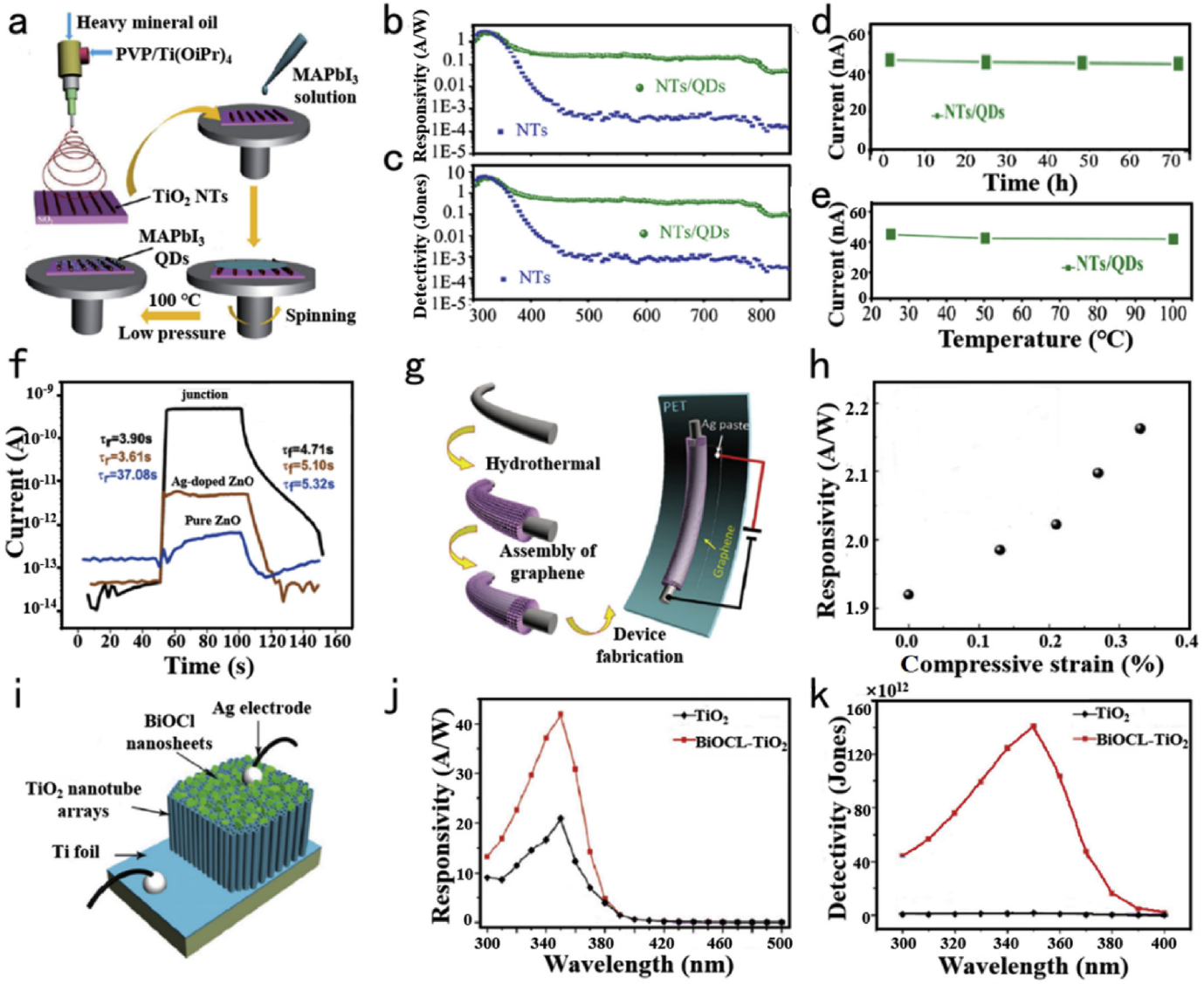

Fig. 3. (**a**) Schematic view for co-electrospinning TiO_2 NTs array and schematic process of spin-coating $MAPbI_3$ QDs on TiO_2 NTs array. (**b**) Logarithmic form of spectroscopic responsivity and (**c**) detectivity under a light with intensity of 26.8 mW/cm^2 for TiO_2 NTs/$MAPbI_3$ QD and TiO_2 NTs, respectively. Photocurrent of TiO_2 NTs/$MAPbI_3$ QDs device which (**d**) was exposed to wet air ranging from 0 to 72 h and (**e**) was exposed to dry air at 25, 50 and 100 °C for 350 nm light illumination. (**f**) Switching characteristics of three devices (pure ZnO and Ag-doped ZnO nanofibers p-n junction, pure ZnO photoconductor, and Ag-doped ZnO photoconductor) at zero bias. (**g**) Device structure of the fiber-shaped ZnO/Graphene PDs. (**h**) The responsivity of the PD under different compressive strain. (**i**) Schematic diagram of the BiOCl–TiO_2 UV PD. (**j**) Responsivity and (k) detectivity versus wavelength of BiOCl–TiO_2 heterojunction PDs.

powered UV-radiation monitor based on a high performance p-CuZnS/n-TiO_2 PD (Xu et al., 2018b), as shown in Fig. 5f and g. The flexible fiber-shaped PD exhibits fast response time of less than 0.2 s, as indicated in Fig. 5h. And the performance remains almost unchanged when it is bent at an angle of 50°, indicating the great potential as wearable electronic devices. Moreover, a maximum responsivity of 2.54 mA/W is obtained at 0 V bias under 300 nm UV illumination (Fig. 5i). As a wearable real-time UV monitor, the optoelectronic characteristic under a small bias were measured, and the results are depicted in Fig. 5j. The fiber-shaped device exhibits an outstanding responsivity of 640 A/W and a high external quantum efficiency of 2.3×10^5% at bias of 3 V, which exhibit the high performance of the flexible and wearable PDs in preventing skin cancer and protecting human health.

Heart rate and blood oxygen saturation are two of the important physiological indexes of human body, the continuous and accurate monitoring can effectively judge the health status of human body and prevent cardiovascular diseases. Pulse oximeter is a non-invasive medical sensing method used to measure pulse rate and arterial blood oxygen saturation (King, 2002). However, the conventional pulse oximeter based on inorganic optoelectronics is limited by the bulk, rigidity and area scaling. The abnormality of heart rate and blood oxygen saturation often occurs suddenly, and wearable pulse oxygen monitoring equipment can obtain the physical sign data of the tested person at any time. To date, the “skin-like” characteristics of wearable devices are proposed (Kim et al., 2016b) and a series of wearable pulse oximeters based on medical PDs have been investigated (Bansal et al., 2015; Lochner et al., 2014; Yokota et al., 2016).

A wearable all-organic pulse oximeter was fabricated, as shown in Fig. 6a, composed of an OLED and a flexible organic PD (OPD), where two OLED arrays and two OPD arrays are placed on opposite sides of a finger. The device can accurately measure pulse rate and oxygenation with errors of 1% and 2%, respectively (Lochner et al., 2014). The performance of OLED and OPD is both crucial to measurement quality of oximeter. Fig. 6b exhibits the OPDs were flexed with radii of around 5 mm and 9 mm, respectively, which represent the wide range of

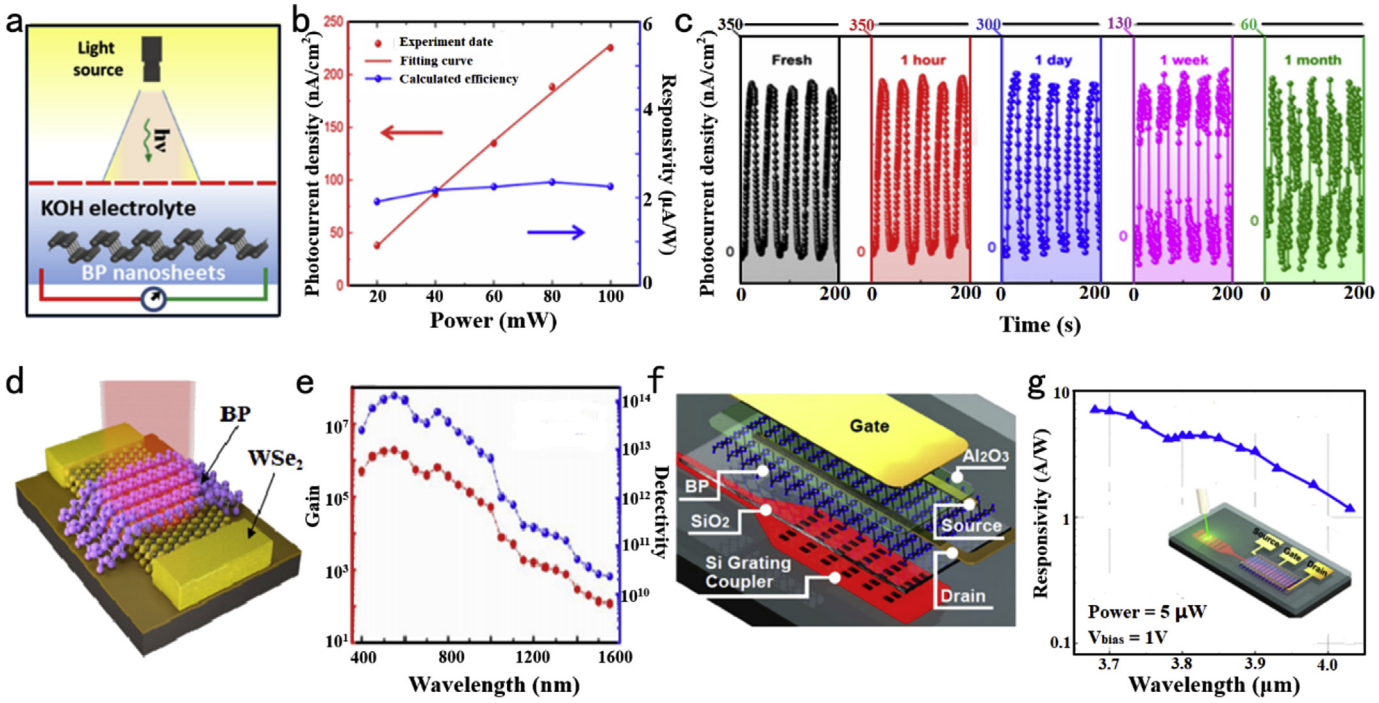

Fig. 4. (**a**) Schematic diagram of the BP nanosheets-based PD. (**b**) Fitting curve and photoconversion efficiencies of BP under various power intensities in 0.1 m KOH. (**c**) Time stability test of BP nanosheets-based PD with time duration of 1 h, 1 day, 1 week, and 1 month in 0.1 m KOH. (**d**) Schematic diagram and optical image of the BP-on-WSe_2 PD with photogate structure. (**e**) The dependence of the photogain and detectivity on the different wavelength illumination at 1 mW/cm^2 incident illumination power density and 0.5 V bias. (**f**) Zoom-in view of the output side of the waveguide-integrated on-chip system with BP-based PD. (**g**) Spectral responsivity of BP-based PD. **Inset**: Schematics of the waveguide-integrated on-chip system with BP-based PD.

human finger sizes, and the ambient noise is reduced by 79% and 93%, respectively. The flexible OPD is able to conform around the human body thus improves the versatility of pulse oximeter.

Tomoyuki et al. prepared ultra-flexible and conformable polymer light-emitting diodes (PLEDs) and OPDs to realize optoelectronic skins (oe-skins) (Yokota et al., 2016), which can be sensed and displayed on the skin surface of human body as shown in Fig. 6c. The device is ultra-thin and ultra-light after combining with an elastomer substrate, showing no performance degradation after 40% compression and 300 times stretching cycles (Fig. 6d and e), indicating its flexible and stability. Furthermore, the device can be used as a reflective pulse oximeter (Fig. 6f) and show good stability in the air (Fig. 6g). Ultimately, flexible organic optical sensors may be directly laminated on organs to monitor the blood oxygen level during and after surgery.

3.2. Implantable biomedical PDs

In the last decade, in addition to wearable PDs, much effort has been devoted to the development of high performance PDs for implantable biomedicine. Retinal prosthetic devices can help patients with age-related macular degeneration and other eye diseases to restore vision through artificial implantation devices physically placed on the retina (Zrenner et al., 1999; Zrenner, 2002; Wang et al., 2012; Chow et al., 2001). However, it is not suitable for long-term use due to the rigidity of the silicon-chip microphotodiode-based implants and the electrode dissolution, resulting subsequent decreased electrical activity (Chow et al., 2001). Ridwan et al. designed and manufactured a flexible and conformable large-format MoS_2/graphene PD on polyimide substrate (Hossain et al., 2017b) (Fig. 7a and b), and then conducted the photoresponse characteristics, biocompatibility and strain-dependent bending test of the device, respectively (Fig. 7d–g). The device shows a high responsivity of 0.3 A/W, which is $\sim 10^3$ times compared to the other reports of heterostructures devices (F et al., 2014; Li et al., 2015). The detectivity is measured to be 3.6×10^{10} Jones, which is comparable to prior reports (Mukherjee et al., 2016). In addition, it shows high biocompatibility with a cell survival rate of up to 98%. This heterostructure still shows a high photo responsivity to incident radiation at a large strain level. These properties pave the way for their future application in retinal prostheses and age-related macular degeneration.

Kang et al. reported PD based on crumpled graphene, which can not only enhance the optical signals, but also have strain-tunable wavelength selectivity (Kang et al., 2016), as shown in Fig. 7h. The crumpled structure lead to increase in areal density of graphene and, thus, the optical absorption. Compared with a flat graphene PD, the textured device exhibited a 400% enhancement in responsivity once the largest crumpling, as shown in Fig. 7i. At the same time, the method is also applicable to other emerging 2D materials, such as MoS_2. Subsequently, the researchers replaced the substrate with silicone-based polymer with high biocompatibility and flexibility, then applied a tensile bending strain of 11.1% to the human brain model (Fig. 7j) and the human heart model (Fig. 7k). It shows that the obtained current-voltage curve is similar to that of the device on the plane (Fig. 7l). In addition, it also shows excellent stability because no degradation of the responsivity was observed over a thousand periods of cyclic tensile strains.

Monitoring of biological activities, such as gene expression (Shavtal et al., 2004), metabolism (Gerich, 2006) and variations in ionic concentration (Grienberger and Konnerth, 2012), can be widely carried out using optical measurement methods. On the one hand, measurement of intrinsic optical signals reflects changes in cell volume (Jentsch, 2016), which can be used to measure blood volume in the brain (Ma et al., 2016) and to track the spread of neuronal excitation, hypoxia, spreading depression (Fayuk et al., 2002). On the other hand, intrinsic optical signals can also provide high resolution for localization of brain activity. Therefore, the device for measuring intrinsic optical signals can be used as an optical sensing platform for studying various physiological and pathological events. Using independent PDs, optical signals are converted into current signals and transmitted directly to the

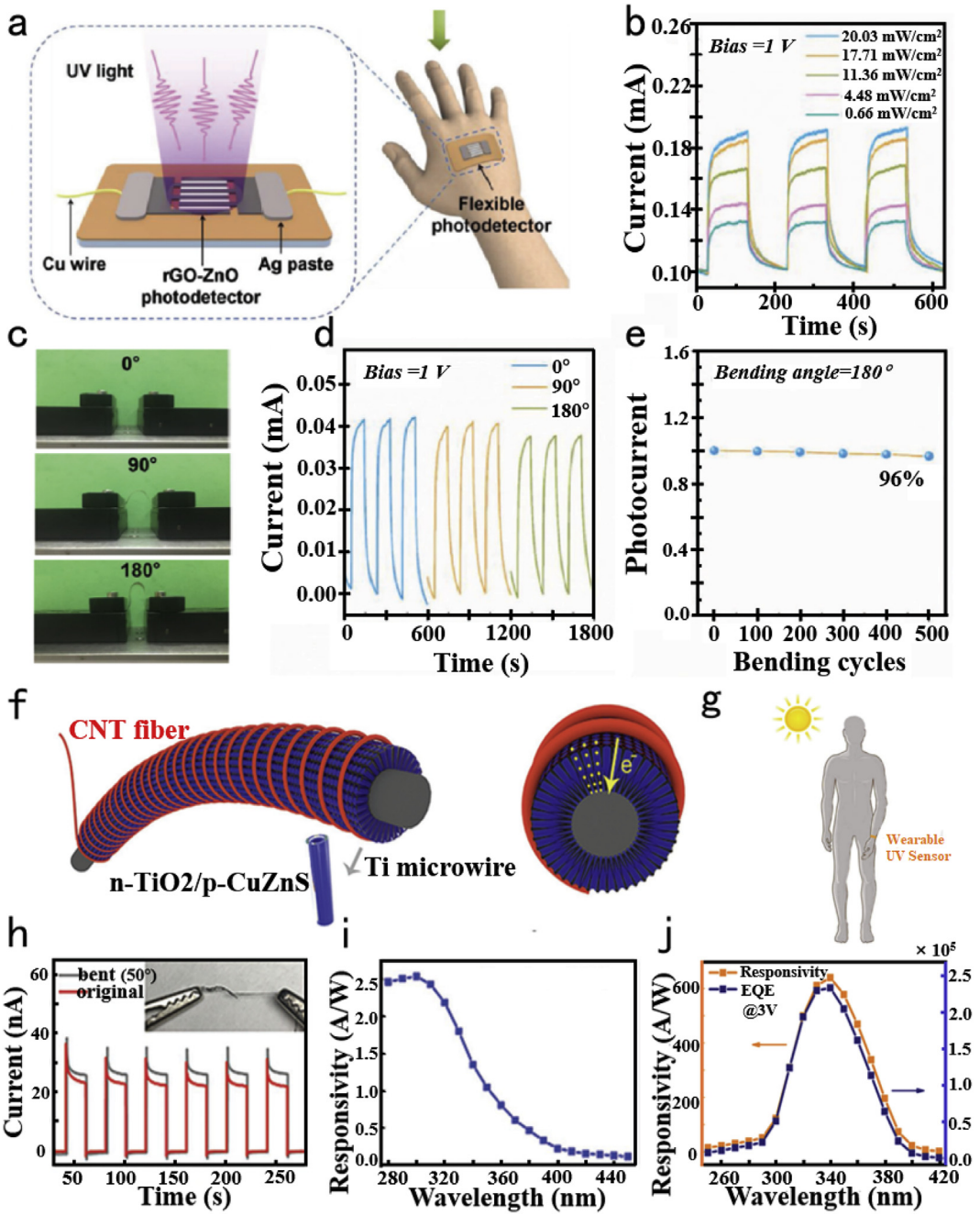

Fig. 5. The wearable UV-radiation monitor based on PDs. (**a**) Schematic diagram of all RGO-ZnO hybrid-based PD. (**b**) Time-resolved photocurrent responses of the PD to different UV illumination intensities. (**c**) Optical images of the flexible PD with bending angle of 0°, 90°, and 180°, respectively. (**d**) Time-resolved photoresponse curves of the device at different bending angles. (**e**) Normalized photocurrent with respect to the bending-unbending cycles at 1 V bias, the bending angle is 180°. (**f**) Schematic diagram of the device configuration of fiber-shaped p-CuZnS/n-TiO_2 nanotube arrays. (**g**) Schematic diagram of the wearable PD as a real-time UV monitor. (**h**) The on-off switching tests of the fiber-shaped PD at the virgin state and bent state (≈50°). (**i**) Responsivity of the fiber-shaped device at zero bias. (**j**) Responsivity and external quantum efficiency of the fiber-shaped PD as a function of wavelength at 3 V.

acquisition system, which provide the possibility to real-time detection of electrical and optical signals under high resolution.

Choi et al. utilized an implanted micro-LEDs optical sensor as a two-way emitter/detectors (Fig. 8a), through measuring localized changes in reflectivity due to cerebral blood flow when attached to the surface of the brain, to detect epileptic seizure events (Choi et al., 2018). The device was fabricated on a 25 μm thick flexible substrate and it was a potential epilepsy research solution that needs to be implanted subcutaneously (Fig. 8b). Based on this, Shahab et al. prepared OPDs with a simple structure (Fig. 8c), serving as a high-sensitivity optical sensor for detecting intrinsic optical signals of living brain tissue (Rezaei-Mazinani et al., 2018). In order to measure real-time changes of intrinsic optical signals in living tissues, a customized device is designed. The brain tissue slices in perfusion bath are provided with electrodes for recording and stimulating electrophysiological activities (Fig. 8d). In the experiment, recording electrode and stimulation electrode were implanted near CA1 and CA3 regions, respectively (Fig. 8e). Firstly, the linear relationship between photocurrent density and optical density in Fig. 8f exhibits high stability during electrophysiological recording time, which is the reliability basis of the optical sensor. Later, OPD detects optical changes during epileptic activity in adult mouse hippocampal slices in Fig. 8g–i. It is proved that the epileptic discharge

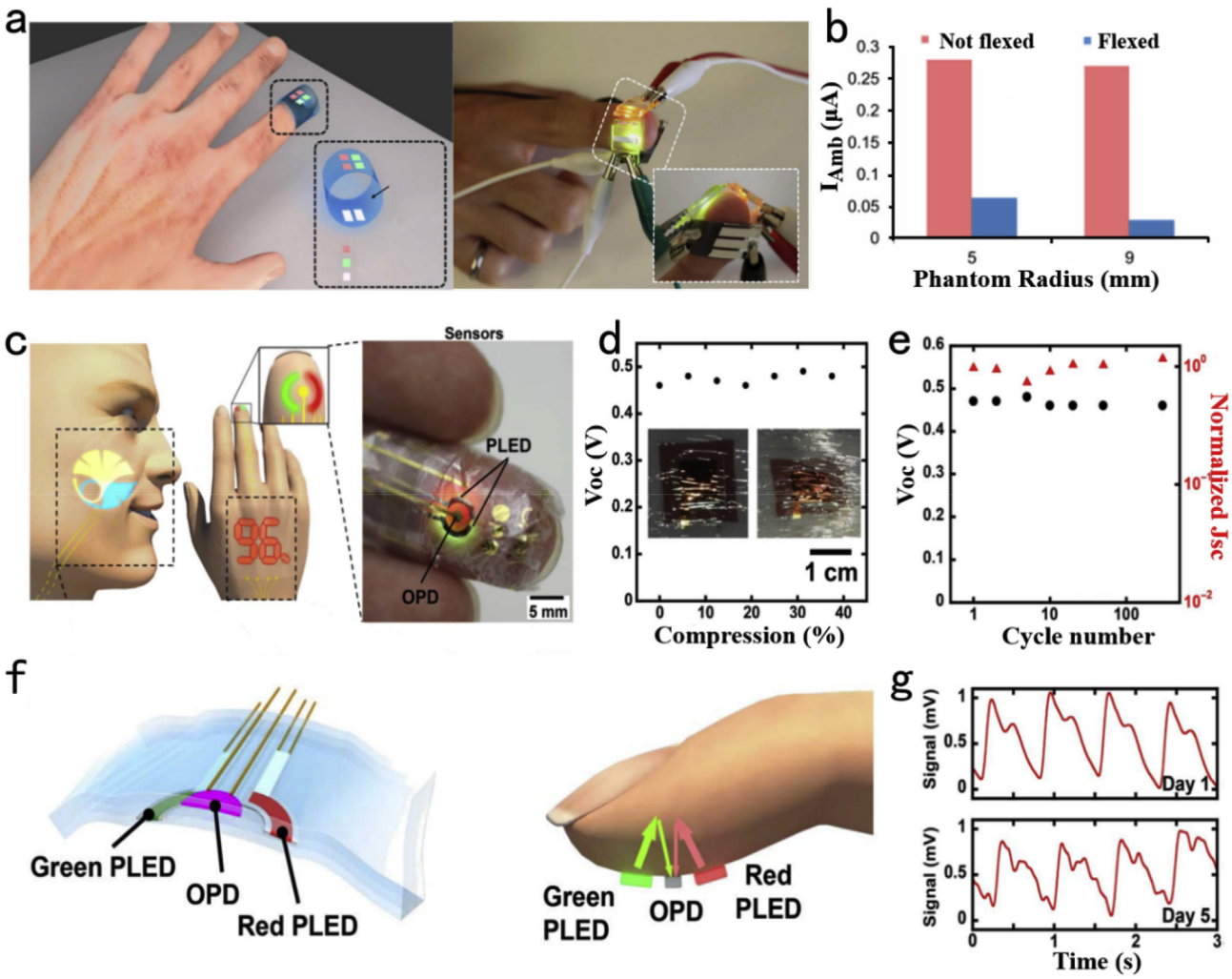

Fig. 6. The wearable pulse oximeter based on PD. (**a**) Pulse oximetry sensor composed of two OLED arrays and two OPDs. (**b**) OPDs were flexed around 5 mm and 9 mm radius phantoms representative of small and large human fingers. (**c**) Schematic diagram of the oe-skins system based on PLED and OPD. (**d**) The open-circuit voltage of the wrinkled OPD. (**e**) Cyclic stretching test of the OPD. (**f**) Device structure of the pulse oximeter and operation principle of the reflective pulse oximeter. (**g**) Air stability of the photoplethysmogram (PPG) signal.

causes significant changes in tissue translucency due to cell swelling and OPD clearly detects this effect, indicating the high feasibility to study typical strong signals (more than 5% optical changes) of pathophysiological events. Then the sensitivity of the device is studied to monitor weak physiological related intrinsic optical signals caused by neuronal activity, as can be seen in Fig. 8j–l. The results show that OPD can simultaneously monitor low and strong amplitude optical signals. Therefore, OPD exhibits high sensitivity and high temporal resolution, providing potential electrophysiological method to detect optical changes in brain tissue.

4. Conclusion and future prospects

This review summarized the research progress and some of the important applications of PDs based on 2D materials in biomedical field. Through the research on robustness, stability and biocompatibility of various devices, PDs based on flexible substrates have been proved to be feasible in wearable devices (such as UV-radiation monitor, pulse oximeter, etc.) and implantable PDs (such as retinal prosthesis, etc.). Despite the tremendous advances in the use of PDs in the biomedical field, there are still many challenges that need to be overcome to develop more accurate and secure systems in real-world applications. Portability and long-term stability, as non-invasive devices, are still challenges in current research of wearable PDs. On the one hand, portable wearable devices need to be further miniaturized to make it possible to integrate into the wearer's daily life. On the other hand, wireless electronic devices need to be integrated to facilitate data processing and secure signal transmission. As invasive PDs, future implantable devices pay more attention to the stability of the long-term implantation and the smaller immune response, ultimately enabling safe and comprehensive medical diagnosis and performance evaluation.

Through the review of the research progress and the applications in biomedical field of PDs based on 2D materials, the importance and existing technical challenges of wearable and implantable photodetectors in biomedical field are understood, showing exciting prospects in this research field. However, most of the researches on the application of PDs in biomedicine, especially implantable devices, up to now have only been proved its feasibility in experimental performance research or theoretical research, but no further research has been done on experimental mice, thus much more research effort is necessary to be conducted before these devices really come into the clinical stage. Therefore, the PDs, especially implanted devices, can be considered for further study *in vivo*, thus taking a step towards clinical application. If all of the above challenges can be overcome, the photodetector can be transferred from the research phase to the clinical phase. Although the research of PDs in biomedicine is still in its infancy, the known

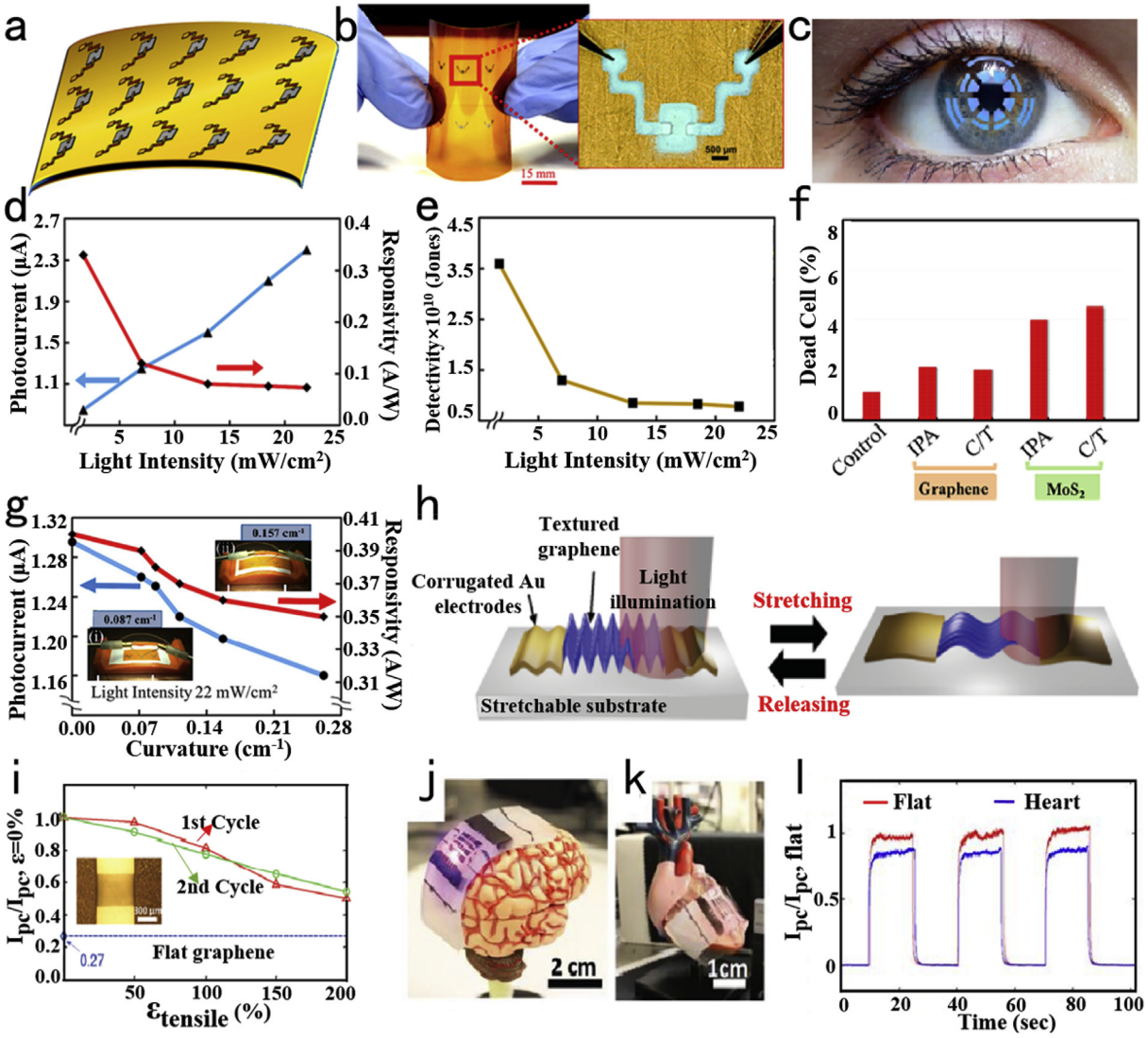

Fig. 7. The implantable PDs. (**a**) 2D MoS_2/graphene heterostructure PDs for resisting age-related macular degeneration printed on flexible substrates. (**b**) An actual array of inkjet printed heterostructure devices on flexible polyimide film. (**c**) Schematic diagram of retinal implant. (**d**) The dependence of photocurrent and responsivity on light intensity. (**e**) Detectivity as a function of light intensity. (**f**) Dead cell percentage of mouse embryonic fibroblasts cells on polyimide substrates. (**g**) Photocurrent and responsivity as a function of curvature to measure the effect of strain at 22 mW/cm^2. **Inset**: Strain-dependent measurements of the devices performed using 3D printed fixtures. (**h**) Schematic diagram of crumpled graphene PD. (**i**) Comparison of measured photocurrent of the textured graphene PD at the varying strains over two cycles and measured photocurrent of a flat graphene PD. **Inset**: Optical microscope image of the textured graphene PD. (**j**) Highly stretchable and conformal PD on the surface of a human brain model. (**k**) PD on the surface of human heart model. (**l**) Dynamic photoresponse of the stretchable PD on the surface of human heart model. Measured photocurrent was normalized with that on flat surface.

outstanding properties of such devices provide excellent impetus for expanding research activities in this fast emerging field. Given the competitive research and huge commercial opportunities for wearable and implantable PDs, they will offer a promising area of research in the coming years. As a result, the market for wearable and implantable PDs is expected to continue to grow rapidly, making health monitoring and disease prevention possible in the near future and continuing to improve people lives.

CRediT authorship contribution statement

Shuangjie Liu: Investigation, Writing - original draft. **Xiao-dong Zhang:** Conceptualization, Supervision, Validation, Writing - review & editing. **Xiaosong Gu:** Supervision, Resources. **Dong Ming:** Formal analysis, Supervision, Validation, Writing - review & editing.

Declaration of competing interest

The authors declare that they have no known competing financial interests or personal relationships that could have appeared to influence the work reported in this paper.

Acknowledgments

This work was supported by the National Natural Science Foundation of China (81971744, 81471786 and U1932107) and the Independent Innovation Foundation of Tianjin University. This work used the Extreme Science and Engineering Discovery Environment (XSEDE), which is supported by the National Science Foundation (ACI-1548562).

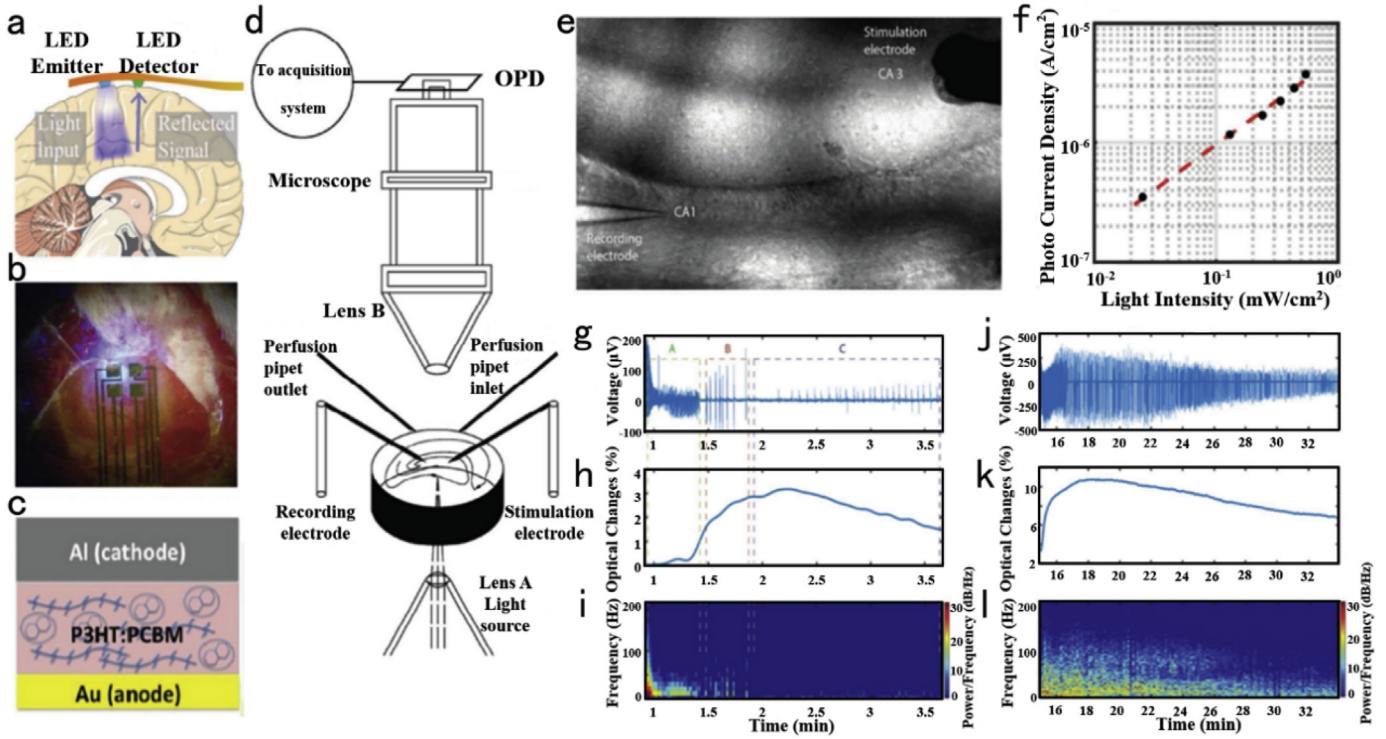

Fig. 8. (**a**) Schematic diagram of an optical recording of intrinsic signals micro-LED device being used to monitor cerebral blood volume. (**b**) Photograph of the micro-LED device implanted on the surface of an exposed brain of a rat. (**c**) Schematic diagram of OPD device structure. (**d**) OPD device experimental setup. The OPD was installed at the optical port in order to detect optical changes. (**e**) Optical image of the hippocampal slice, where the overall optical activity of the neuronal network was recorded. (**f**) Linear dynamic range (log scale) in response to the illumination intensity range used for the electrophysiological recordings. (**g**) OPD detects optical changes with the same temporal resolution as simultaneously recordings electrophysiological signals during pathological epileptiform activity. (**h**) OPD generated current expressed as a percentage of the baseline value. (**i**) Spectrotemporal representation of the local field potential change illustrated in panel (**h**). (**j**) Local field potential responses to 10 Hz electrical stimulation for 30 and 10 s recorded in hippocampal slice of adult mouse brain. (**k**) Responses to both stimulation events were accompanied by changes in the electrical current generated by the OPD. (**l**) Time-frequency-power presentation of the local field potential signals during and after the first cycle of synaptic activation.

References

Ajayan, P., Kim, P., Banerjee, K., 2016. Two-dimensional van der Waals materials. Phys. Today 69, 38–44.

Alsaif, M.M., Kuriakose, S., Walia, S., Syed, N., Jannat, A., Zhang, B.Y., Haque, F., Mohiuddin, M., Alkathiri, T., Pillai, N., 2019. 2D SnO/In_2O_3 van der Waals heterostructure photodetector based on printed oxide skin of liquid metals. Adv. Mater. Interfaces 6, 1900007.

An, J., Le, T.D., Lim, C.H.J., Tran, V.T., Zhan, Z., Gao, Y., Zheng, L., Sun, G., Kim, Y.J., 2018. Single-step selective laser writing of flexible photodetectors for wearable optoelectronics. Adv. Sci. 5, 1800496.

Araki, H., Kim, J., Zhang, S., Banks, A., Crawford, K.E., Sheng, X., Gutruf, P., Shi, Y., Pielak, R.M., Rogers, J.A., 2016. Materials and device designs for an epidermal UV colorimetric dosimeter with near field communication capabilities. Adv. Funct. Mater. 27, 1604465.

Bansal, A.K., Hou, S., Kulyk, O., Bowman, E.M., Samuel, I.D., 2015. Wearable organic optoelectronic sensors for medicine. Adv. Mater. 27, 7638–7644.

Bao, Q., Zhang, H., Yang, J.X., Wang, S., Tang, D.Y., Jose, R., Ramakrishna, S., Lim, C.T., Loh, K.P., 2010. Ultrafast photonics: graphene-polymer nanofiber membrane for ultrafast photonics. Adv. Funct. Mater. 20, 782–791.

Boruah, B.D., Ferry, D.B., Mukherjee, A., Misra, A., 2015. Few-layer graphene/ZnO nanowires based high performance UV photodetector. Nanotechnology 26, 235703.

Boruah, B.D., Mukherjee, A., Misra, A., 2016. Sandwiched assembly of ZnO nanowires between graphene layers for a self-powered and fast responsive ultraviolet photodetector. Nanotechnology 27, 095205.

Buscema, M., Groenendijk, D.J., Blanter, S.I., Steele, G.A., Zant, H.S.J.V.D., Castellanos-Gomez, A., 2014. Fast and broadband photoresponse of few-layer black phosphorus field-effect transistors. Nano Lett. 14, 3347–3352.

Buscema, M., Island, J.O., Groenendijk, D.J., Blanter, S.I., Steele, G.A., Van, d.Z., Herre, S.J., Castellanos-Gomez, A., 2015. ChemInform abstract: photocurrent generation with two-dimensional van der Waals semiconductors. Chem. Soc. Rev. 44, 3691–3718.

Cao, F., Meng, L., Wang, M., Tian, W., Li, L., 2019. Gradient energy band driven high--performance self-powered perovskite/CdS photodetector. Adv. Mater. 31, 1806725.

Chang, H., Sun, Z., Yuan, Q., Ding, F., Tao, X., Yan, F., Zheng, Z., 2010. Thin film field-effect phototransistors from bandgap-tunable, solution-processed, few-layer reduced graphene oxide films. Adv. Mater. 22, 4872–4876.

Chang, H., Sun, Z., Saito, M., Yuan, Q., Zhang, H., Li, J., Wang, Z., Fujita, T., Ding, F., Zheng, Z., 2013. Regulating infrared photoresponses in reduced graphene oxide phototransistors by defect and atomic structure control. ACS Nano 7, 6310–6320.

Chen, Y., Tan, C., Zhang, H., Wang, L., 2015a. Two-dimensional graphene analogues for biomedical applications. Chem. Soc. Rev. 44, 2681–2701.

Chen, X., Wu, Y., Wu, Z., Han, Y., Xu, S., Wang, L., Ye, W., Han, T., He, Y., Cai, Y., 2015b. High-quality sandwiched black phosphorus heterostructure and its quantum oscillations. Nat. Commun. 6, 7315.

Chen, X., Yang, H., Liu, G., Feng, G., Dai, M., Hu, Y., Chen, H., Cao, W., Hu, P.A., Hu, W., 2018. Hollow spherical nanoshell arrays of 2D layered semiconductor for high-performance photodetector device. Adv. Funct. Mater. 28, 1705153.

Cheng, C., Yang, H., Huang, B., Zhang, H., Fan, H., Zhang, X., Mao, X., Fui, Q., Yang, X., Pei, W., Chen, H., 2019. Performance enhancement of graphene photodetectors via in situ preparation of TiO_2 on graphene channels. Adv. Mater. Technol. 4, 1800548.

Chitara, B., Panchakarla, L.S., Krupanidhi, S.B., Rao, C.N., 2011a. Infrared photodetectors based on reduced graphene oxide and graphene nanoribbons. Adv. Mater. 23, 5419–5424.

Chitara, B., Panchakarla, L.S., Krupanidhi, S.B., Rao, C.N., 2011b. Infrared photodetectors based on reduced graphene oxide and graphene nanoribbons. Adv. Mater. 23, 5419–5424.

Chiu, K.L., Xu, Y., 2017. Single-electron transport in graphene-like nanostructures. Phys. Rep. 669, 1–42.

Choi, C., Colón-Berríos, A.R., Hamachi, L.S., Owen, J.S., Schwartz, T.H., Ma, H., Kymissis, I., 2018. Localizing seizure activity in the brain using implantable micro-LEDs with quantum dot downconversion. Adv. Mater. Technol. 3, 1700366.

Chong, H., Wei, G., Hou, H., Yang, H., Shang, M., Gao, F., Yang, W., Shen, G., 2015. High-performance solar-blind ultraviolet photodetector based on electrospun TiO_2-$ZnTiO_3$ heterojunction nanowires. Nano Res 8, 2822–2832.

Chow, A.Y., Pardue, M.T., Chow, V.Y., Peyman, G.A., Liang, C., Perlman, J.I., Peachey, N.S., 2001. Implantation of silicon chip microphotodiode arrays into the cat subretinal space. IEEE Trans. Rehabil. Eng. 9, 86–95.

Craciun, M.F., Russo, S., Yamamoto, M., Tarucha, S., 2011. Tuneable electronic properties in graphene. Nano Today 6, 42–60.

Dang, V.Q., Trung, T.Q., Kim, D.I., Duy le, T., Hwang, B.U., Lee, D.W., Kim, B.Y., Toan le, D., Lee, N.E., 2015. Ultrahigh responsivity in graphene-ZnO nanorod hybrid UV photodetector. Small 11, 3054–3065.

De, F.D., Goykhman, I., Yoon, D., Bruna, M., Eiden, A., Milana, S., Sassi, U., Barbone, M., Dumcenco, D., Marinov, K., 2016. High responsivity, large-area graphene/MoS_2

flexible photodetectors. ACS Nano 10, 8252.
Deng, Y., Luo, Z., Conrad, N.J., Liu, H., Gong, Y., Najmaei, S., Ajayan, P.M., Lou, J., Xu, X., Ye, P.D., 2014. Black phosphorus-monolayer MoS_2 van der Waals heterojunction p-n diode. ACS Nano 8, 8292–8299.
Devan, R.S., Patil, R.A., Lin, J.H., Ma, Y.R., 2012. One-dimensional metal-oxide nanostructures: recent developments in synthesis, characterization, and applications. Adv. Funct. Mater. 22, 3326–3370.
Dhanabalan, S.C., Ponraj, J.S., Zhang, H., Bao, Q., 2016. Present perspectives of broadband photodetectors based on nanobelts, nanoribbons, nanosheets and the emerging 2D materials. Nanoscale 8, 6410–6434.
Ding, Y., Zhou, N., Gan, L., Yan, X., Wu, R., Abidi, I.H., Waleed, A., Pan, J., Ou, X., Zhang, Q., Zhuang, M., Wang, P., Pan, X., Fan, Z., Zhai, T., Luo, Z., 2018. Stacking-mode confined growth of 2H-$MoTe_2$/MoS_2 bilayer heterostructures for UV-vis-IR photodetectors. Nano Energy 49, 200–208.
Duan, L., He, F., Tian, Y., Sun, B., Fan, J., Yu, X., Ni, L., Zhang, Y., Chen, Y., Zhang, W., 2017. Fabrication of self-powered fast-response ultraviolet photodetectors based on graphene/ZnO:Al nanorod-array-film structure with stable Schottky barrier. ACS Appl. Mater. Interfaces 9, 8161–8168.
Echtermeyer, T.J., Nene, P.S., Trushin, M., Gorbachev, R.V., Eiden, A.L., Milana, S., Sun, Z., Schliemann, J., Lidorikis, E., Novoselov, K.S., Ferrari, A.C., 2014. Photothermoelectric and photoelectric contributions to light detection in metal-graphene-metal photodetectors. Nano Lett. 14, 3733–3742.
F, W., H, Y., L, B., AP, R., E, L., A, F., CR, W., V, S.R., T, G., A, E., 2014. Heterostructures produced from nanosheet-based inks. Nano Lett. 14, 3987–3992.
Fang, X., Hu, L., Huo, K., Gao, B., Zhao, L., Liao, M., Chu, P.K., Bando, Y., Golberg, D., 2011. New ultraviolet photodetector based on individual Nb_2O_5 nanobelts. Adv. Funct. Mater. 21, 3907–3915.
Fang, J., Wang, D., Devault, C., Chung, T.F., Chen, Y.P., Boltasseva, A., Shalaev, V.M., Kildishev, A.V., 2017. In Enhanced graphene photodetector with fractal metasurface. Nano Lett. 17, 57–62.
Fayuk, D., Aitken, P.G., Somjen, G.G., Turner, D.A., 2002. Two different mechanisms underlie reversible, intrinsic optical signals in rat hippocampal slices. J. Neurophysiol. 87, 1924–1937.
Gao, L., Zhang, Y., Malyarchuk, V., Jia, L., Jang, K.I., Webb, R.C., Fu, H., Shi, Y., Zhou, G., Shi, L., 2015. Epidermal photonic devices for quantitative imaging of temperature and thermal transport characteristics of the skin. Nat. Commun. 5, 4938.
Geim, A.K., Grigorieva, I.V., 2013. Van der Waals heterostructures. Nature 499, 419–425.
Gerich, F.J., 2006. Optical and pharmacological tools to investigate the role of mitochondria during oxidative stress and neurodegeneration. Prog. Neurobiol. 79, 136–171.
Gomathi, P.T., Sahatiya, P., Badhulika, S., 2017. Large-area, flexible broadband photodetector based on ZnS-MoS_2 hybrid on paper substrate. Adv. Funct. Mater. 27, 1701611.
Grienberger, C., Konnerth, A., 2012. Imaging calcium in neurons. Neuron 73, 862–885.
Guo, X., Wang, W., Nan, H., Yu, Y., Jiang, J., Zhao, W., Li, J., Zafar, Z., Xiang, N., Ni, Z., 2016. High-performance graphene photodetector by interfacial gating. Optica 3, 1066–1070.
Gupta, A., Sakthivel, T., Seal, S., 2015. Recent development in 2D materials beyond graphene. Prog. Mater. Sci. 73, 44–126.
Hafeez, M., Gan, L., Li, H., Ma, Y., Zhai, T., 2016. Large-area bilayer ReS_2 film/multilayer ReS_2 flakes synthesized by chemical vapor deposition for high performance photodetectors. Adv. Funct. Mater. 26, 4551–4560.
He, T., Zhang, X., Ding, X., Sun, C., Zhao, Y., Yu, Q., Ning, J., Wang, R., Yu, G., Lu, S., Zhang, K., Zhang, X., Zhang, B., 2019. Broadband ultraviolet photodetector based on vertical Ga_2O_3/GaN nanowire array with high responsivity. Adv. Optical Mater. 7, 1801563.
Heikenfeld, J., Jajack, A., Feldman, B., Granger, S., Gaitonde, S., Begtrup, G., Katchman, B., 2019. Accessing analytes in biofluids for peripheral biochemical monitoring. Nat. Biotechnol. 37, 407–419.
Hossain, R.F., Deaguero, I.G., Boland, T., Kaul, A.B., 2017a. Biocompatible, large-format, inkjet printed heterostructure MoS_2-graphene photodetectors on conformable substrates. NPJ 2D Mater. Appl. 1.
Hossain, R.F., Deaguero, I.G., Boland, T., Kaul, A.B., 2017b. Biocompatible, large-format, inkjet printed heterostructure MoS_2-graphene photodetectors on conformable substrates. NPJ 2D Mater. Appl. 1.
Hsu, C.Y., Lien, D.H., Lu, S.Y., Chen, C.Y., Kang, C.F., Chueh, Y.L., Hsu, W.K., He, J.H., 2012. Supersensitive, ultrafast, and broad-band light-harvesting scheme employing carbon nanotube/TiO_2 core–shell nanowire geometry. ACS Nano 6, 6687–6692.
Hua, X., Juanxia, W., Qingliang, F., Nannan, M., Chunming, W., Jin, Z., 2014. High responsivity and gate tunable graphene-MoS_2 hybrid phototransistor. Small 10, 2300–2306.
Huang, Y., Zhuge, F., Hou, J., Lv, L., Luo, P., Zhou, N., Gan, L., Zhai, T., 2018. Van der Waals coupled organic molecules with monolayer MoS_2 for fast response photodetectors with gate-tunable responsivity. ACS Nano 12, 4062–4073.
Huang, L., Dong, B., Guo, X., Chang, Y., Chen, N., Huang, X., Liao, W., Zhu, C., Wang, H., Lee, C., Ang, K.W., 2019. Waveguide-integrated black phosphorus photodetector for mid-infrared applications. ACS Nano 13, 913–921.
Huo, N., Gupta, S., Konstantatos, G., 2017. MoS_2-HgTe quantum dot hybrid photodetectors beyond 2 microm. Adv. Mater. 29, 1606576.
Jariwala, D., Marks, T.J., Hersam, M.C., 2017. Mixed-dimensional van der Waals heterostructures. Nat. Mater. 16, 170–181.
Jentsch, T.J., 2016. VRACs and other ion channels and transporters in the regulation of cell volume and beyond. Nat. Rev. Mol. Cell Biol. 17, 293–307.
Jin, H., Abu-Raya, Y.S., Haick, H., 2017. Advanced materials for health monitoring with skin-based wearable devices. Adv. Healthc. Mater. 6, 1700024.
Kang, K., Xie, S., Huang, L., Han, Y., Huang, P.Y., Mak, K.F., Kim, C.J., Muller, D., Park, J., 2015. High-mobility three-atom-thick semiconducting films with wafer-scale homogeneity. Nature 520, 656–660.
Kang, P., Wang, M.C., Knapp, P.M., Nam, S., 2016. Crumpled graphene photodetector with enhanced, strain-tunable, and wavelength-selective photoresponsivity. Adv. Mater. 28, 4639–4645.
Khodkov, T., Withers, F., Christopher Hudson, D., Felicia Craciun, M., Russo, S., 2012. Electrical transport in suspended and double gated trilayer graphene. Appl. Phys. Lett. 100, 013114.
Kim, J., Salvatore, G.A., Araki, H., Chiarelli, A.M., Xie, Z., Banks, A., Sheng, X., Liu, Y., Lee, J.W., Jang, K.I., 2016a. Battery-free, stretchable optoelectronic systems for wireless optical characterization of the skin. Sci. Adv. 2, e1600418.
Kim, J., Salvatore, G.A., Araki, H., Chiarelli, A.M., Xie, Z., Banks, A., Sheng, X., Liu, Y., Lee, J.W., Jang, K.I., Heo, S.Y., Cho, K., Luo, H., Zimmerman, B., Kim, J., Yan, L., Feng, X., Xu, S., Fabiani, M., Gratton, G., Huang, Y., Paik, U., Rogers, J.A., 2016b. Battery-free, stretchable optoelectronic systems for wireless optical characterization of the skin. Sci. Adv. 2, e1600418.
Kim, J., Campbell, A.S., Ávila, B., Wang, J., 2019. Wearable biosensors for healthcare monitoring. Nat. Biotechnol. 37, 389–406.
King, P., 2002. Design of pulse oximeters. IEEE Eng. Med. Biol. 17, 117.
Konstantatos, G., Badioli, M., Gaudreau, L., Osmond, J., Bernechea, M., Arquer, F.P.G.D., Gatti, F., Koppens, F.H.L., 2011. Hybrid graphene-quantum dot phototransistors with ultrahigh gain. Nat. Nanotechnol. 7, 363–368.
Kuc, A., Zibouche, N., Heine, T., 2011. Influence of quantum confinement on the electronic structure of the transition metal sulfide TS_2. Phys. Rev. B 83, 2237–2249.
Kwak, J.Y., Hwang, J., Calderon, B., Alsalman, H., Spencer, M.G., 2016. Long wavelength optical response of graphene-MoS_2 heterojunction. Appl. Phys. Lett. 108, 091108.
Leung, S., Ho, K., Kung, P., Hsiao, V., Alshareef, H., Wang, Z., He, J., 2018. A self-powered and flexible organometallic halide perovskite photodetector with very high detectivity. Adv. Mater. 30, 1704611.
Li, X., Zhu, H., 2016. The graphene–semiconductor Schottky junction. Phys. Today 69, 46–51.
Li, X., Wang, X., Zhang, L., Lee, S., Dai, H., 2008. Chemically derived, ultrasmooth graphene nanoribbon semiconductors. Science 319, 1229–1232.
Li, L., Yu, Y., Ye, G.J., Ge, Q., Ou, X., Wu, H., Feng, D., Chen, X.H., Zhang, Y., 2014. Black phosphorus field-effect transistors. Nat. Nanotechnol. 9, 372–377.
Li, J., Naiini, M.M., Vaziri, S., Lemme, M.C., Östling, M., 2015. Inkjet printing of MoS_2. Adv. Funct. Mater. 24, 6524–6531.
Li, X., Zhu, M., Du, M., Lv, Z., Zhang, L., Li, Y., Yang, Y., Yang, T., Li, X., Wang, K., 2016. High detectivity graphene-silicon heterojunction photodetector. Small 12, 595–601.
Li, Z., Hui, Q., Guo, Z., Ren, X., Huang, Z., Xiang, Q., Dhanabalan, S.C., Ponraj, J.S., Du, Z., Li, J., 2017a. High-performance photo-electrochemical photodetector based on liquid-exfoliated few-layered InSe nanosheets with enhanced stability. Adv. Funct. Mater. 28, 1705237.
Li, X., Tao, L., Chen, Z., Fang, H., Li, X., Wang, X., Xu, J.-B., Zhu, H., 2017b. Graphene and related two-dimensional materials: structure-property relationships for electronics and optoelectronics. Appl. Phys. Rev. 4, 021306.
Li, Z., Wang, L., Wu, S., Zhang, G., Meng, M., Ma, X., 2017c. Photoelectric characteristics of Eu～(3＋)-Doped MoS_2 thin films. Micronanoelectron. Technol. 54, 390–395.
Li, A., Chen, Q., Wang, P., Gan, Y., Qi, T., Wang, P., Tang, F., Wu, J., Chen, R., Zhang, L., Gong, Y., 2019a. Ultrahigh-sensitive broadband photodetectors based on dielectric shielded $MoTe_2$/graphene/SnS_2 p-g-n junctions. Adv. Mater. 31, 1805656.
Li, M., Yu, M., Su, D., Zhang, J., Jiang, S., Wu, J., Wang, Q., Liu, S., 2019b. Ultrahigh responsivity UV photodetector based on Cu nanostructure/ZnO QD hybrid architectures. Small 15, 1901606.
Lin, C., Sun, D., Lin, Y., Tsai, T., Cheng, C., Sun, W., Ko, F., 2017. A flexible and miniaturized hair dye based photodetector via chemiluminescence pathway. Biosens. Bioelectron. 90, 349–355.
Ling, X., Huang, S., Hasdeo, E.H., Liang, L., Parkin, W.M., Tatsumi, Y., Nugraha, A.R., Puretzky, A.A., Masih, D.P., Sumpter, B.G., 2016. Correction to anisotropic electron-photon and electron-phonon interactions in black phosphorus. Nano Lett. 16, 2260–2267.
Liu, C.H., Chang, Y.C., Norris, T.B., Zhong, Z., 2014a. Graphene photodetectors with ultra-broadband and high responsivity at room temperature. Nat. Nanotechnol. 9, 273–278.
Liu, H., Neal, A.T., Zhu, Z., Luo, Z., Xu, X., Tománek, D., Ye, P.D., 2014b. Phosphorene: an unexplored 2D semiconductor with a high hole mobility. ACS Nano 8, 4033–4041.
Liu, Y., Wang, F., Wang, X., Wang, X., Flahaut, E., Liu, X., Li, Y., Wang, X., Xu, Y., Shi, Y., Zhang, R., 2015a. Planar carbon nanotube-graphene hybrid films for high-performance broadband photodetectors. Nat. Commun. 6, 8589.
Liu, X., Ji, X., Liu, M., Liu, N., Tao, Z., Dai, Q., Wei, L., Li, C., Zhang, X., Wang, B., 2015b. High-performance Ge quantum dot decorated graphene/zinc-oxide heterostructure infrared photodetector. ACS Appl. Mater. Interfaces 7, 2452–2458.
Liu, Y., Weiss, N.O., Duan, X., Cheng, H.C., Huang, Y., Duan, X., 2016. Van der Waals heterostructures and devices. Nat. Rev. Mater. 1, 16042.
Liu, Y., Huang, W., Chen, W., Wang, X., Guo, J., Tian, H., Zhang, H., Wang, Y., Yu, B., Ren, T.-L., 2019a. Plasmon resonance enhanced WS_2 photodetector with ultra-high sensitivity and stability. Appl. Surf. Sci. 481, 1127–1132.
Liu, X., Sun, G., Chen, P., Liu, J., Zhang, Z., Li, J., Ma, H., Zhao, B., Wu, R., Dang, W., Liu, Y., Duan, X., 2019b. High-performance asymmetric electrodes photodiode based on Sb/WSe_2 heterostructure. Nano Res 12, 339–344.
Lochner, C.M., Khan, Y., Pierre, A., Arias, A.C., 2014. All-organic optoelectronic sensor for pulse oximetry. Nat. Commun. 5, 5745.
Long, M., Wang, Y., Wang, P., Zhou, X., Xia, H., Luo, C., Huang, S., Zhang, G., Yan, H., Fan, Z., 2019. Palladium diselenide long-wavelength infrared photodetector with high sensitivity and stability. ACS Nano 13, 2511–2519.
Lu, X., Jiang, P., Bao, X., 2019. Phonon-enhanced photothermoelectric effect in SrTiO 3

ultra-broadband photodetector. Nat. Commun. 10, 138.
Ma, Y., Shaik, M.A., Kozberg, M.G., Kim, S.H., Portes, J.P., Timerman, D., Hillman, E.M., 2016. Resting-state hemodynamics are spatiotemporally coupled to synchronized and symmetric neural activity in excitatory neurons. Proc. Natl. Acad. Sci. U.S.A. 113, E8463.
Mingjin, D., Hongyu, C., Rui, F., Wei, F., Yunxia, H., Huihui, Y., Guangbo, L., Xiaoshuang, C., Jia, Z., Cheng-Yan, X., 2018. A dual-band multilayer InSe self-powered photodetector with high performance induced by surface plasmon resonance and asymmetric Schottky junction. ACS Nano 12, 8739–8747.
Mukherjee, S., Maiti, R., Katiyar, A.K., Das, S., Ray, S.K., 2016. Novel colloidal MoS_2 quantum dot heterojunctions on silicon platforms for multifunctional optoelectronic devices. Sci. Rep. 6, 29016.
Narayanan, D.L., Rao, N.S., Fox, J.L., 2010. Review: ultraviolet radiation and skin cancer. Int. J. Dermatol. 49, 978–986.
Ning, Y., Zhang, Z., Teng, F., Fang, X., 2018a. Novel transparent and self-powered UV photodetector based on crossed ZnO nanofiber array homojunction. Small 14, 1703754.
Ning, Y., Zhang, Z., Teng, F., Fang, X., 2018b. Novel transparent and self-powered UV photodetector based on crossed ZnO nanofiber array homojunction. Small 14, 1703754.
Novoselov, K.S., Geim, A.K., Morozov, S.V., Jiang, D., Zhang, Y., Dubonos, S.V., Grigorieva, I.V., Firsov, A.A., 2004. Electric field effect in atomically thin carbon films. Science 306, 666–669.
Novoselov, K.S., Mishchenko, A., Carvalho, A., Castro Neto, A.H., 2016. 2D materials and van der Waals heterostructures. Science 353, aac9439.
Ohta, T., Bostwick, A., Seyller, T., Horn, K., Rotenberg, E., 2006. Controlling the electronic structure of bilayer graphene. Science 313, 951–954.
Oriol, L.S., Dominik, L., Metin, K., Aleksandra, R., Andras, K., 2013. Ultrasensitive photodetectors based on monolayer MoS_2. Nat. Nanotechnol. 8, 497–501.
Ouyang, W., Teng, F., Jiang, M., Fang, X., 2017. ZnO film UV photodetector with enhanced performance: heterojunction with $CdMoO_4$ microplates and the hot electron injection effect of Au nanoparticles. Small 13, 1702177.
Ouyang, W., Teng, F., Fang, X., 2018. High performance BiOCl nanosheets/TiO_2 nanotube Arrays heterojunction UV photodetector: the influences of self-induced inner electric fields in the BiOCl nanosheets. Adv. Funct. Mater. 28, 1707178.
Pak, Y., Park, W., Mitra, S., Sasikala Devi, A.A., Loganathan, K., Kumaresan, Y., Kim, Y., Cho, B., Jung, G.Y., Hussain, M.M., Roqan, I.S., 2018. Enhanced performance of MoS_2 photodetectors by inserting an ALD-processed TiO_2 interlayer. Small 14, 1703176.
Patel, D.B., Chauhan, K.R., Park, S.H., Kim, J., 2017. High-performing transparent photodetectors based on Schottky contacts. Mater. Sci. Semicond. Process. 64, 137–142.
Patil, V., Capone, A., Strauf, S., Yang, E.H., 2013. Improved photoresponse with enhanced photoelectric contribution in fully suspended graphene photodetectors. Sci. Rep. 3, 2791.
Poya, Y., Bijandra, K., Tara, F., Canhui, W., Mohammad, A., David, T., J Ernesto, I., Klie, R.F., Amin, S.K., 2015. High-quality black phosphorus atomic layers by liquid-phase exfoliation. Adv. Mater. 27, 1887–1892.
Pumera, M., Loo, A.H., 2014. Layered transition-metal dichalcogenides (MoS_2 and WS_2) for sensing and biosensing. Trends Anal. Chem. 61, 49–53.
Ren, X., Li, Z., Huang, Z., Sang, D., Qiao, H., Qi, X., Li, J., Zhong, J., Zhang, H., 2017. Environmentally robust black phosphorus nanosheets in solution: application for self-powered photodetector. Adv. Funct. Mater. 27, 1606834.
Rezaei-Mazinani, S., Ivanov, A.I., Proctor, C.M., Gkoupidenis, P., Bernard, C., Malliaras, G.G., Ismailova, E., 2018. Monitoring intrinsic optical signals in brain tissue with organic photodetectors. Adv. Mater. Technol. 3, 1700333.
Sabu, C., Henna, T.K., Raphey, V.R., Nivitha, K.P., Pramod, K., 2019. Advanced biosensors for glucose and insulin. Biosens. Bioelectron. 141.
Schwartz, G., Tee, B.C.K., Mei, J., Appleton, A.L., Kim, D.H., Wang, H., Bao, Z., 2013. Flexible polymer transistors with high pressure sensitivity for application in electronic skin and health monitoring. Nat. Commun. 4, 1859.
Shavtal, Y., Singer, R.H., Darzacq, X., 2004. Imaging gene expression in single living cells. Nat. Rev. Mol. Cell Biol. 10, 855–861.
Shen, Y., Yang, S., Zhou, P., Sun, Q., Wang, P., Wan, L., Li, J., Chen, L., Wang, X., Ding, S., 2013. Evolution of the band-gap and optical properties of graphene oxide with controllable reduction level. Carbon 62, 157–164.
Splendiani, A., Sun, L., Zhang, Y., Li, T., Kim, J., Chim, C.Y., Galli, G., Wang, F., 2010. Emerging photoluminescence in monolayer MoS_2. Nano Lett. 10, 1271–1275.
Sun, Z., Chang, H., 2014. Graphene and graphene-like two-dimensional materials in photodetection: mechanisms and methodology. ACS Nano 8, 4133–4156.
Sun, Q., Miao, H., Hu, X., Zhang, G., Zhang, D., Liu, E., Hao, Y., Liu, X., Fan, J., 2016. Preparation of MoS_2/RGO nano heterojunction and photoelectric property. J. Mater. Sci. Mater. Electron. 27, 1–7.
Tan, H., Fan, Y., Zhou, Y., Chen, Q., Xu, W., Warner, J.H., 2016. Ultrathin 2D photodetectors utilizing chemical vapor deposition grown WS_2 with graphene electrodes. ACS Nano 10, 7866–7873.
Tan, H., Xu, W., Sheng, Y., Lau, C.S., Fan, Y., Chen, Q., Tweedie, M., Wang, X., Zhou, Y., Warner, J.H., 2017. Lateral graphene-contacted vertically stacked WS_2/MoS_2 hybrid photodetectors with large gain. Adv. Mater. 29, 1702917.
Tian, H., Fan, C., Liu, G., Yuan, S., Zhang, Y., Wang, M., Li, E., 2019. Ultrafast broadband photodetector based on SnS synthesized by hydrothermal method. Appl. Surf. Sci. 487, 1043–1048.
Tongay, S., Suh, J., Ataca, C., Fan, W., Luce, A., Kang, J.S., Liu, J., Ko, C., Raghunathanan, R., Zhou, J., 2013. Defects activated photoluminescence in two-dimensional semiconductors: interplay between bound, charged, and free excitons. Sci. Rep. 3, 2657.
Velický, M., Bissett, M.A., Woods, C.R., Toth, P.S., Georgiou, T., Kinloch, I.A., Novoselov, K.S., Dryfe, R.A., 2016. Correction to photoelectrochemistry of pristine mono- and few-layer MoS_2. Nano Lett. 16, 2023–2032.
Vellampatti, S., Reddeppa, M., Dugasani, S., Mitta, S., Gnapareddy, B., Kim, M., Park, S., 2019. High performance UV photodetectors using Nd^{3+} and Er^{3+} single- and co-doped DNA thin films. Biosens. Bioelectron. 126, 44–50.
Wang, F., Zhang, Y., Tian, C., Girit, C., Zettl, A., Crommie, M., Shen, Y.R., 2008. Gate-variable optical transitions in graphene. Science 320, 206–209.
Wang, L., Mathieson, K., Kamins, T.I., Loudin, J.D., Galambos, L., Goetz, G., Sher, A., Mandel, Y., Huie, P., Lavinsky, D., 2012. Photovoltaic retinal prosthesis: implant fabrication and performance. J. Neural Eng. 9, 046014.
Wang, X., Yang, G., Xiong, Z., Zheng, C., Zhang, T., 2014. Silk-molded flexible, ultrasensitive, and highly stable electronic skin for monitoring human physiological signals. Adv. Mater. 26, 1336–1342.
Wang, L., Jie, J., Shao, Z., Zhang, Q., Zhang, X., Wang, Y., Sun, Z., Lee, S.T., 2015a. MoS_2/Si heterojunction with vertically standing layered structure for ultrafast, high-detectivity, self-driven visible–near infrared photodetectors. Adv. Funct. Mater. 25, 2910–2919.
Wang, F., Wang, Z., Xu, K., Wang, F., Wang, Q., Huang, Y., Yin, L., He, J., 2015b. Tunable GaTe-MoS_2 van der Waals p-n junctions with novel optoelectronic performance. Nano Lett. 15, 7558–7566.
Wang, Y., Fullon, R., Acerce, M., Petoukhoff, C.E., Yang, J., Chen, C., Du, S., Lai, S.K., Lau, S.P., Voiry, D., O'Carroll, D., Gupta, G., Mohite, A.D., Zhang, S., Zhou, H., Chhowalla, M., 2017. Solution-Processed MoS_2/organolead trihalide perovskite photodetectors. Adv. Mater. 29, 1603995.
Wang, P., Wang, Y., Ye, L., Wu, M., Xie, R., Wang, X., Chen, X., Fan, Z., Wang, J., Hu, W., 2018. Ferroelectric localized field-enhanced ZnO nanosheet ultraviolet photodetector with high sensitivity and low dark current. Small 14, 1800492.
Weinan, Z., Yogeesh, M.N., Shixuan, Y., Aldave, S.H., Joon-Seok, K., Sushant, S., Li, T., Nanshu, L., Deji, A., 2015. Flexible black phosphorus ambipolar transistors, circuits and AM demodulator. Nano Lett. 15, 1883–1890.
Wen, Y., Yin, L., He, P., Wang, Z., Zhang, X., Wang, Q., Shifa, T.A., Xu, K., Wang, F., Zhan, X., Wang, F., Jiang, C., He, J., 2016. Integrated high-performance infrared phototransistor arrays composed of nonlayered PbS-MoS_2 heterostructures with edge contacts. Nano Lett. 16, 6437–6444.
Withers, F., Bointon, T.H., Craciun, M.F., Russo, S., 2013. All-graphene photodetectors. ACS Nano 7, 5052–5057.
Xiang, D., Han, C., Wu, J., Zhong, S., Liu, Y., Lin, J., Zhang, X.A., Ping, H.W., B, Ö., Neto, A.H., 2015. Surface transfer doping induced effective modulation on ambipolar characteristics of few-layer black phosphorus. Nat. Commun. 6, 6485.
Xiao, P., Mao, J., Ding, K., Luo, W., Hu, W., Zhang, X., Zhang, X., Jie, J., 2018. Solution-Processed 3D RGO-MoS_2/pyramid Si heterojunction for ultrahigh detectivity and ultra-broadband photodetection. Adv. Mater. 30, 1801729.
Xu, M., Liang, T., Shi, M., Chen, H., 2013. Graphene-like two-dimensional materials. Chem. Rev. 113, 3766–3798.
Xu, Z.Q., Zhang, Y., Wang, Z., Shen, Y., Huang, W., Xia, X., Yu, W., Xue, Y., Sun, L., Zheng, C., 2016a. Atomically thin lateral p-n junction photodetector with large effective detection area. 2D Mater. 3, 041001.
Xu, Y., Yuan, J., Fei, L., Wang, X., Bao, Q., Wang, Y., Zhang, K., Zhang, Y., 2016b. Selenium-doped black phosphorus for high-responsivity 2D photodetectors. Small 12, 5000–5007.
Xu, H., Han, X., Dai, X., Liu, W., Wu, J., Zhu, J., Kim, D., Zou, G., Sablon, K.A., Sergeev, A., Guo, Z., Liu, H., 2018a. High detectivity and transparent few-layer MoS_2/glassy-graphene heterostructure photodetectors. Adv. Mater. 30, 1706561.
Xu, X., Chen, J., Cai, S., Long, Z., Zhang, Y., Su, L., He, S., Tang, C., Liu, P., Peng, H., Fang, X., 2018b. A real-time wearable UV-radiation monitor based on a high-performance p-CuZnS/n-TiO_2 photodetector. Adv. Mater. 30, e1803165.
Yang, Y., Gao, W., 2018. Wearable and flexible electronics for continuous molecular monitoring. Chem. Soc. Rev. 48.
Yang, G.H., Shi, J.J., Wang, S., Xiong, W.W., Jiang, L.P., Burda, C., Zhu, J.J., 2013. Fabrication of a boron nitride-gold nanocluster composite and its versatile application for immunoassays. Chem. Commun. 49, 10757–10759.
Yang, F., Zheng, M., Zhao, L., Guo, J., Zhang, B., Gu, G., Cheng, G., Du, Z., 2019. The high-speed ultraviolet photodetector of ZnO nanowire Schottky barrier based on the triboelectric-nanogenerator-powered surface-ionic-gate. Nano Energy 60, 680–688.
Ye, L., Wang, P., Luo, W., Gong, F., Liao, L., Liu, T., Tong, L., Zang, J., Xu, J., Hu, W., 2017. Highly polarization sensitive infrared photodetector based on black phosphorus-on-WSe_2 photogate vertical heterostructure. Nano Energy 37, 53–60.
Yokota, T., Zalar, P., Kaltenbrunner, M., Jinno, H., Matsuhisa, N., Kitanosako, H., Tachibana, Y., Yukita, W., Koizumi, M., Someya, T., 2016. Ultraflexible organic photonic skin. Sci. Adv. 2, e1501856.
Yu, T., Wang, F., Xu, Y., Ma, L., Pi, X., Yang, D., 2016. Graphene coupled with silicon quantum dots for high-performance bulk-silicon-based Schottky-junction photodetectors. Adv. Mater. 28, 4912–4919.
Yu, W., Li, S., Zhang, Y., Ma, W., Sun, T., Yuan, J., Fu, K., Bao, Q., 2017. Near-infrared photodetectors based on $MoTe_2$/graphene heterostructure with high responsivity and flexibility. Small 13, 1700268.
Yu, X., Li, Y., Hu, X., Zhang, D., Tao, Y., Liu, Z., He, Y., Haque, M.A., Liu, Z., Wu, T., Wang, Q.J., 2018. Narrow bandgap oxide nanoparticles coupled with graphene for high performance mid-infrared photodetection. Nat. Commun. 9, 4299.
Yuan, H., Liu, X., Afshinmanesh, F., Li, W., Xu, G., Sun, J., Lian, B., Curto, A.G., Ye, G., Hikita, Y., 2015. Polarization-sensitive broadband photodetector using a black phosphorus vertical p-n junction. Nat. Nanotechnol. 156–158, 707–713.
Yun, W.S., Han, S.W., Hong, S.C., Kim, I.G., Lee, J.D., 2012. Thickness and strain effects on electronic structures of transition metal dichalcogenides: 2H-MX_2 semiconductors (M = Mo, W; X = S, Se, Te). Phys. Rev. B Condens. Matter 85, 033305.
Zeng, L.H., Wu, D., Lin, S.H., Xie, C., Yuan, H.Y., Lu, W., Lau, S.P., Chai, Y., Luo, L.B., Li, Z.J., 2018. Controlled synthesis of 2D palladium diselenide for sensitive photodetector applications. Adv. Funct. Mater. 29, 1806878.

Zhang, W., Demarteau, M., Hoffmann, A., Dubey, M., Roelofs, A., 2014a. Tunable transport gap in phosphorene. Nano Lett. 14, 5733–5739.
Zhang, W., Chuu, C.P., Huang, J.K., Chen, C.H., Tsai, M.L., Chang, Y.H., Liang, C.T., Chen, Y.Z., Chueh, Y.L., He, J.H., 2014b. Ultrahigh-gain photodetectors based on atomically thin graphene-MoS_2 heterostructures. Sci. Rep. 4, 3826.
Zhang, Y., Liu, J., Wang, Z., Xue, Y., Ou, Q., Polavarapu, L., Zheng, J., Qi, X., Bao, Q., 2016a. Synthesis, properties, and optical applications of low-dimensional perovskites. Chem. Commun. 52, 13637–13655.
Zhang, Y., Yu, Y., Mi, L., Wang, H., Zhu, Z., Wu, Q., Zhang, Y., Jiang, Y., 2016b. In situ fabrication of vertical multilayered MoS_2/Si homotype heterojunction for high-speed visible-near-infrared photodetectors. Small 12, 1062–1071.
Zhang, D.Y., Ge, C.W., Wang, J.Z., Zhang, T.F., Wu, Y.C., Liang, F.X., 2016c. Single-layer graphene-TiO_2 nanotubes array heterojunction for ultraviolet photodetector application. Appl. Surf. Sci. 387, 1162–1168.
Zhang, Y., Xu, J., Shi, S., Gao, Y., Zhao, X., Wei, C., Zhang, X., Li, L., 2017. Photoelectric response properties under UV/Red light irradiation of ZnO nanorod arrays coated with vertically aligned MoS_2 nanosheets. Nanotechnology 28, 415202.
Zhao, Q., Guo, Y., Zhou, Y., Yan, X., Xu, X., 2017. Solution-processable exfoliation and photoelectric properties of two-dimensional layered MoS_2 photoelectrodes. J. Colloid Interface Sci. 490, 287–293.
Zheng, Z., Zhuge, F., Wang, Y., Zhang, J., Gan, L., Zhou, X., Li, H., Zhai, T., 2017. Decorating perovskite quantum dots in TiO_2 nanotubes array for broadband response photodetector. Adv. Funct. Mater. 27, 1703115.
Zhu, C., Du, D., Lin, Y., 2015. Graphene and graphene-like 2D materials for optical biosensing and bioimaging: a review. 2D Mater. 2, 032004.
Zhu, C., Du, D., Lin, Y., 2017. Graphene-like 2D nanomaterial-based biointerfaces for biosensing applications. Biosens. Bioelectron. 89, 43–55.
Zhu, Z., Wang, S., Zhu, Y., Liu, X., Zou, Y., Gu, Y., Ju, D., Zeng, H., 2018. Fiber-shaped ZnO/graphene Schottky photodetector with strain effect. Adv. Mater. Interfaces 5, 1800136.
Zrenner, E., 2002. Will retinal implants restore vision? Science 295, 1022–1025.
Zrenner, E., Stett, A., Weiss, S., Aramant, R.B., Guenther, E., Kohler, K., Miliczek, K.D., Seiler, M.J., Haemmerle, H., 1999. Can subretinal microphotodiodes successfully replace degenerated photoreceptors? Vis. Res. 39, 2555–2567.